Applied Catalysis B: Environmental 142–143 (2013) 861–876

Contents lists available at SciVerse ScienceDirect

Applied Catalysis B: Environmental

journal homepage: www.elsevier.com/locate/apcatb

Experimental and modeling study of a dual-layer (SCR + PGM) NH_3 slip monolith catalyst (ASC) for automotive SCR aftertreatment systems. Part 1. Kinetics for the PGM component and analysis of SCR/PGM interactions

Massimo Colombo[a], Isabella Nova[a], Enrico Tronconi[a,*], Volker Schmeißer[b], Brigitte Bandl-Konrad[b], Lisa Zimmermann[c]

[a] Dipartimento di Energia, Laboratorio di Catalisi e Processi Catalitici, Politecnico di Milano, Piazza Leonardo da Vinci 32, I-20133 Milano, Italy
[b] Daimler AG, 019-G206 RD/RPE, 70546 Stuttgart, Germany
[c] Daimler AG, 019-D121 TP/PME, 70546 Stuttgart, Germany

ARTICLE INFO

Article history:
Received 28 July 2012
Received in revised form 17 October 2012
Accepted 29 October 2012
Available online 12 November 2012

Keywords:
Urea SCR
Ammonia slip
ASC
Zeolite catalysts
Diesel exhaust aftertreatment

ABSTRACT

We present herein the first of two parts in the development and validation of a chemically and physically consistent mathematical model of a commercial dual-layer (SCR + PGM) monolithic NH_3 slip converter (ASC). The overall project followed a systematic approach of growing complexity, and its results emphasize the beneficial features of a dual-layer configuration with the SCR catalyst on top of the PGM component. Specifically, we report in this paper $NH_3/O_2/NO—NO_2$ steady-state and transient kinetic runs performed over the PGM component of the dual-layer NH_3 slip catalyst. The PGM component was tested in a representative temperature range (150–550 °C) in the form of precursor washcoat powders at high space velocities in order to gain kinetic information. From these data an original global PGM kinetic model was developed, which fully accounts for the effects of temperature and of NO_2/NO_x feed ratio (0–1) on NH_3 oxidation. The model considers NO_2 inhibition on NO oxidation, as well as a novel NO_2 inhibition effect on the NH_3 oxidation reactions. Comparative $NH_3/O_2/NO—NO_2$ steady-state runs were performed also over two combinations of SCR + PGM powders (sequential double-bed and mechanical mixture). The N_2 selectivity was greater over the mechanical mixture, as in this configuration the unselective NH_3 oxidation products (NO_x) formed over the PGM catalyst had a chance to further react selectively with NH_3 over the SCR catalyst. Such a positive interaction between the PGM and the SCR catalytic chemistries was satisfactorily predicted by a model involving the simple superposition of the PGM and SCR kinetics. In the following part of the project the herein developed PGM kinetics, together with consistent SCR kinetics, will be incorporated in a novel dual-layer monolith catalyst model and validated against both lab-scale and engine test bench data collected over dual-layer ASC systems.

1. Introduction

To meet current and future vehicle emission regulations like EURO VI and Tier 2, the application of exhaust aftertreatment systems is needed in addition to engine internal measures [1]. Selective catalytic reduction by NH_3 (NH_3-SCR) has become an established process to reduce NO_x emissions from lean exhaust gas (e.g. diesel exhausts) from passenger cars as well as from light- and heavy-duty vehicles. The reducing agent NH_3 is generated on board from an aqueous urea solution (AdBlue®), carried in a separate tank and injected into the exhaust gas upstream of the SCR catalyst. NH_3 is adsorbed onto the SCR catalyst and then converted by NO_x reduction reactions. The injected amount of AdBlue® must be controlled depending on the operating conditions in order to sustain high levels of NH_3 adsorption and of De-NO_x conversion. At the same time, NH_3 emissions from the aftertreatment system into the environment must be avoided. For this purpose a so called NH_3 slip catalyst (ASC) is more and more frequently introduced in modern exhaust gas aftertreatment (EGA) systems, often as a small monolith slice after the SCR unit, with the purpose of oxidizing unreacted NH_3 leaving the SCR brick [2].

Platinum and other precious metals (PGM) are typically adopted as very active elements for NH_3 oxidation [10]. However, they also exhibit a poor selectivity to N_2, i.e. the desired final product. As a solution, it has been shown that the combination of a PGM-based washcoat with a SCR washcoat according to a dual-layer architecture is beneficial regarding both conversion and selectivity performances [11]. Specifically, if the SCR layer is placed on top of the oxidation layer, we can expect in principle an increase of the N_2 selectivity. In fact, NO_x formed by unselective NH_3 oxidation

* Corresponding author. Tel.: +39 02 2399 3264; fax: +39 02 2399 3318.
E-mail address: enrico.tronconi@polimi.it (E. Tronconi).

0926-3373/$ – see front matter © 2012 Elsevier B.V. All rights reserved.
http://dx.doi.org/10.1016/j.apcatb.2012.10.031

Nomenclature

C_i	gas-phase concentration of species i [mol/m^3 gas]
E_j	rate parameter for T-dependence of reaction j [K]
k°_j	logarithm of rate constant of reaction j at Tref [–]
$k_{\text{ads-PGM}}$	rate constant for NH_3 adsorption [1/s]
K_{NN}	rate parameter in (Eq. (16)) [m^3/mol]
K_{NO}	rate parameter in (Eq. (17)) [m^3/mol]
K_{NHNOOX}	rate parameter in (Eq. (18)) [m^3/mol]
$K_{\text{NO}_2\text{-PGM}}$	rate parameter in (Eq. (19)) [m^3/mol]
$K^{\text{eq}}_{\text{NO}_2}$	equilibrium constant of reaction (R.4) [1/bar$^{0.5}$]
P_{O_2}	partial pressure of O_2 [bar]
Q	flow rate [m^3/s]
R	ideal gas constant [J/mol K]
R_i	rate of formation of ith species [mol/m$^3_{\text{cat}}$ s]
r_k	rate of reaction k [mol/m$^3_{\text{cat}}$ s]
T	temperature [K]
Tref	reference temperature [K]
v	gas linear velocity [m/s]
V_{CAT}	volume of catalyst bed [m^3]
z	reactor axial coordinate [m]

Greek symbols

α	molar feed ratio between NH_3 and NO_x [–]
ε	void fraction of catalyst bed [–]
θ_j^{PGM}	surface coverage of adsorbed species j on PGM catalyst [–]
θ_j^{SCR}	surface coverage of adsorbed species j on SCR catalyst [–]
$\nu_{i,k}$	stoichiometric coefficient of species i in reaction k
χ	volumetric fraction of PGM catalyst in mechanical mixture [–]
Ω_j^{PGM}	PGM catalyst: adsorption capacity of species j [mol/m$^3_{\text{cat}}$]
Ω_j^{SCR}	SCR catalyst: adsorption capacity of species j [mol/m$^3_{\text{cat}}$]

in the PGM layer must diffuse back through the SCR layer above, where they can be selectively converted by the residual NH_3 to nitrogen. Thus, such a particular SCR-ASC system enables minimal NH_3 breakthrough at increased NH_3 and NO_x conversions.

With such a high degree of complexity of modern EGA systems, modeling plays an important role as part of the global automotive development process. The physico-chemical processes on the SCR catalyst are already well understood and modeled [3–9], whereas this is not the case for the ASC, for which only a few literature reports exist [2,10] wherein its functionality has been investigated and mathematically described in order to enable the simulation of vehicle tailpipe emissions. Particularly, modeling of the dual-layer ASC configuration requires a dedicated study of the processes prevailing in each single washcoat layer (SCR + PGM), as well as a suitable structure of the converter model in order to describe related synergetic effects. Whereas 1D models of single-layer washcoated catalysts are common in the SCR literature, modeling of dual-layer washcoats has been rarely published so far.

The present paper reports part of a systematic work aimed at the development of a chemically consistent mathematic model of dual-layer ASC converters. A preliminary step involved the catalytic activity study and the kinetic modeling of the SCR component in the ASC system [3], namely a state-of-the-art Fe-zeolite SCR catalyst. This paper deals with the second step of the model development: the NH_3 oxidation over the PGM component of the ASC system was herein studied under typical automotive conditions (e.g. in a representative T-range and in the presence of NO_x, including NO_2) in order to develop a dedicated global kinetic model. In addition, the potential synergies of the catalytic chemistries associated with the PGM and the SCR active phases were also investigated by comparing two different reactor configurations, involving either the sequential arrangement of the two catalysts in a double-bed configuration, or their intimate mixing in a mechanical mixture. Finally, the last stage of the project, to be reported in a forthcoming companion publication, will involve the integration of the SCR/PGM kinetic models in a specifically developed mathematical model of dual-layer monolithic catalysts [12], followed by the lab-scale and full-scale validation of the developed mathematical model against data collected over the single layered SCR and PGM monoliths, as well as over the full dual-layer ASC monolith catalyst.

2. Methods

2.1. Experimental

The commercial dual-layer ASC system herein studied was composed of state-of-the-art PGM and SCR catalysts: the PGM catalyst was a Pt/Al_2O_3-based system, while a Fe-zeolite was used as NH_3-SCR catalyst component. The original ASC system was a dual-layer monolith with an SCR layer coated on top of a PGM one; for the present study however the two catalysts were supplied in the form of precursor powders of the monolith washcoats.

Kinetic runs were carried out in a flow-microreactor consisting of a quartz tube (6 mm i.d.) placed in an electric oven. Three different reactors were prepared for the present study: one was loaded with the PGM catalyst only, while two others were loaded with both SCR and PGM catalysts. In the latter case two different configurations were studied, named in the following as "Double Bed" and "Mechanical Mixture" configuration. In the case of the Double Bed configuration two consecutive catalyst beds were loaded in the microreactor, where the SCR catalytic bed was followed by a PGM layer, as shown in Fig. 1A. On the opposite, the Mechanical Mixture configuration involved the intimate mixing of the two powders into a single catalytic bed, as illustrated in Fig. 1B. In both the "Double Bed" and "Mechanical Mixture" configurations the amount of PGM catalyst loaded in the reactor was the same and equal to that loaded in the case of runs over the PGM catalyst only, while the relative proportion of the two catalysts was representative of typical SCR/PGM washcoat load ratios in dual-layer ASC monoliths.

In all cases before being loaded in the reactor the catalyst powders were dried and sieved (140–200 mesh), and diluted with pure cordierite powders up to a total load of 160 mg, which provided an acceptable depth of the catalytic bed and, at the same time, prevented bypass. The reactor outlet was directly connected to a quadrupole mass spectrometer (Balzers QMS 200, for analysis of N_2O and N_2) and, in parallel, to a UV-analyzer (ABB LIMAS 11HW, for analysis of NO, NO_2 and NH_3). NH_3, NO, NO_2, N_2O, O_2 and He were dosed from bottled calibrated gas mixtures by mass flow controllers, while water vapor was added by means of a saturator. The catalyst temperature was measured by a K-type thermocouple immersed in the catalyst bed. In the case of the Double Bed configuration the thermocouple was immersed in the SCR catalyst bed: based on independent diagnostic measurements of the temperature profile along the axial direction of the reactor, we assumed the same temperature also for the following PGM layer, being both layers placed within the isothermal zone of the oven.

The catalysts were pre-conditioned in a T-ramp at 5 °C/min up to 600 °C in 8% O_2 (v/v) and 8% H_2O (v/v) followed by hold at 600 °C for 5 h. Kinetic runs included mainly isothermal steady-state experiments performed in the 150–550 °C temperature range. At steady state conditions the N-balance always closed within ±10%, consistently with the accuracy of the analysis apparatus.

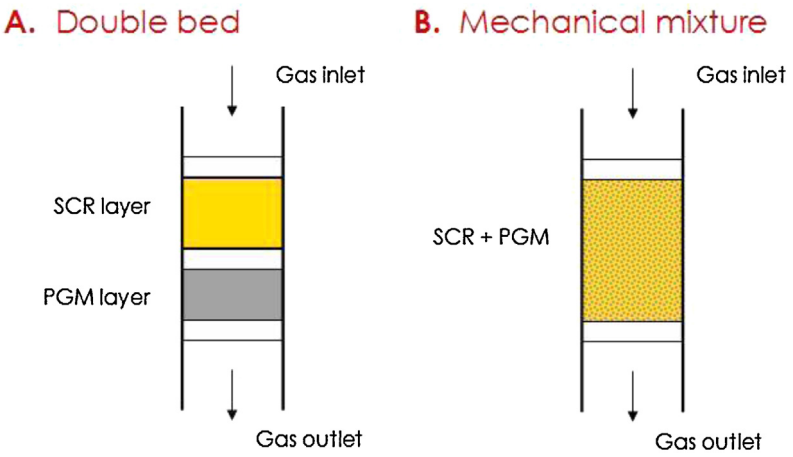

Fig. 1. Tested configurations of SCR/PGM combined systems.

The NH_3 adsorption/desorption on the PGM catalytic system was instead studied by isothermal Transient Response (TRM) runs (NH_3 step feed) followed by Temperature Programmed Desorption (TPD) experiments. Typical feed concentrations of NO_x and NH_3 ranged between 0 and 1000 ppm, always in the presence of O_2 (8%, v/v), H_2O (8%, v/v) and balance He. The system was operated at atmospheric pressure with a Gas Hourly Space Velocity (GHSV) in the range 325,000–1,093,000 $cm^3/h\,g_{cat}$ (STP). A detailed description of the experimental equipment and procedures can be found elsewhere [13].

Experimental results are frequently presented in the paper in terms of NH_3 conversion and products yields, calculated according to the following equations:

$$NH_3\ \text{conversion} = \frac{\left[NH_3^{in}\right] - \left[NH_3^{out}\right]}{\left[NH_3^{in}\right]} \cdot 100 \quad (1)$$

$$N_2\ \text{yield} = \frac{2 \cdot \left[N_2^{out}\right]}{\left[NH_3^{in}\right] + \left[NO_x^{in}\right]} \cdot 100 \quad (2)$$

$$NO_x\ \text{yield} = \frac{\left[NO_x^{out}\right]}{\left[NH_3^{in}\right] + \left[NO_x^{in}\right]} \cdot 100 \quad (3)$$

$$N_2O\ \text{yield} = \frac{2 \cdot \left[N_2O^{out}\right]}{\left[NH_3^{in}\right] + \left[NO_x^{in}\right]} \cdot 100 \quad (4)$$

2.2. Reactor model

In analogy with the approach used for the SCR component of the ASC [3], experimental data collected over the powdered PGM catalyst have been analyzed according to a heterogeneous one-dimensional dynamic plug-flow reactor model, assuming the catalyst bed to be isothermal and isobaric.

The model is based upon the following unsteady material balance differential equations for gaseous and adsorbed species [14]:

$$\text{gaseous phase}: \quad \varepsilon \frac{\partial C_i}{\partial t} = -v \frac{\partial C_i}{\partial z} + (1-\varepsilon) R_i \quad (5)$$

$$\text{adsorbed phase}: \quad \Omega_j \frac{\partial \theta_i}{\partial t} = R_i \quad (6)$$

where ε = void fraction of catalyst bed (−); C_i = gas-phase concentration of ith species (mol/m^3); v = gas linear velocity (m/s); z = reactor axial coordinate (m); R_i = rate of formation of ith species, computed according to:

$$R_i = \sum_{k=1}^{NR} r_k \cdot v_{i,k} \quad (7)$$

where r_k is the rate of reaction k and $v_{i,k}$ is the stoichiometric coefficient of species i in reaction k;

Ω_j = catalyst adsorption capacity of adsorbed species j (mol/m$^3_{cat}$);

θ_j = surface coverage of adsorbed species j (−).

The rate parameters included in the adopted reaction rates were estimated by global multiresponse non-linear regressions based on the least squares method. For this purpose the BURENL routine, developed by Prof. Guido Buzzi-Ferraris, has been used [15,16].

As described in the "Methods" section, the interaction between SCR and PGM components of the ASC system was studied in two different reactor configurations named "Double Bed" and "Mechanical Mixture". PGM/SCR "Double Bed" reactor simulations were based on the sequential implementation of SCR and PGM kinetics within the just described reactor model, where the SCR kinetics were those published in [3]. In view of the arrangement of the catalytic beds (SCR catalyst followed by the PGM catalyst), the output of the SCR layer simulation was used as the input for the simulation with the PGM model.

On the opposite, the simulation of the kinetic data collected over the SCR/PGM "Mechanical Mixture" configuration called for a dedicated model accounting for the simultaneous presence of two different active phases in different amounts. Again, a heterogeneous one-dimensional plug-flow dynamic reactor model that assumes the catalytic bed to be isothermal and isobaric has been employed. Perfect mixing and homogeneous distribution of the two active phases were assumed, resulting in the following unsteady differential material balance equations for adsorbed and gaseous species:

$$\text{SCR adsorbed phase}: \quad \Omega_j^{SCR} \frac{\partial \theta_j^{SCR}}{\partial t} = -(1-\chi) \cdot R_j^{SCR} \quad (8)$$

$$\text{PGM adsorbed phase}: \quad \Omega_j^{PGM} \frac{\partial \theta_j^{PGM}}{\partial t} = -\chi \cdot R_j^{PGM} \quad (9)$$

$$\text{Gas phase}: \quad \varepsilon \frac{\partial C_i}{\partial t} = -v \cdot \frac{\partial C_i}{\partial z} + (1-\varepsilon) R_i^{TOT} \quad (10)$$

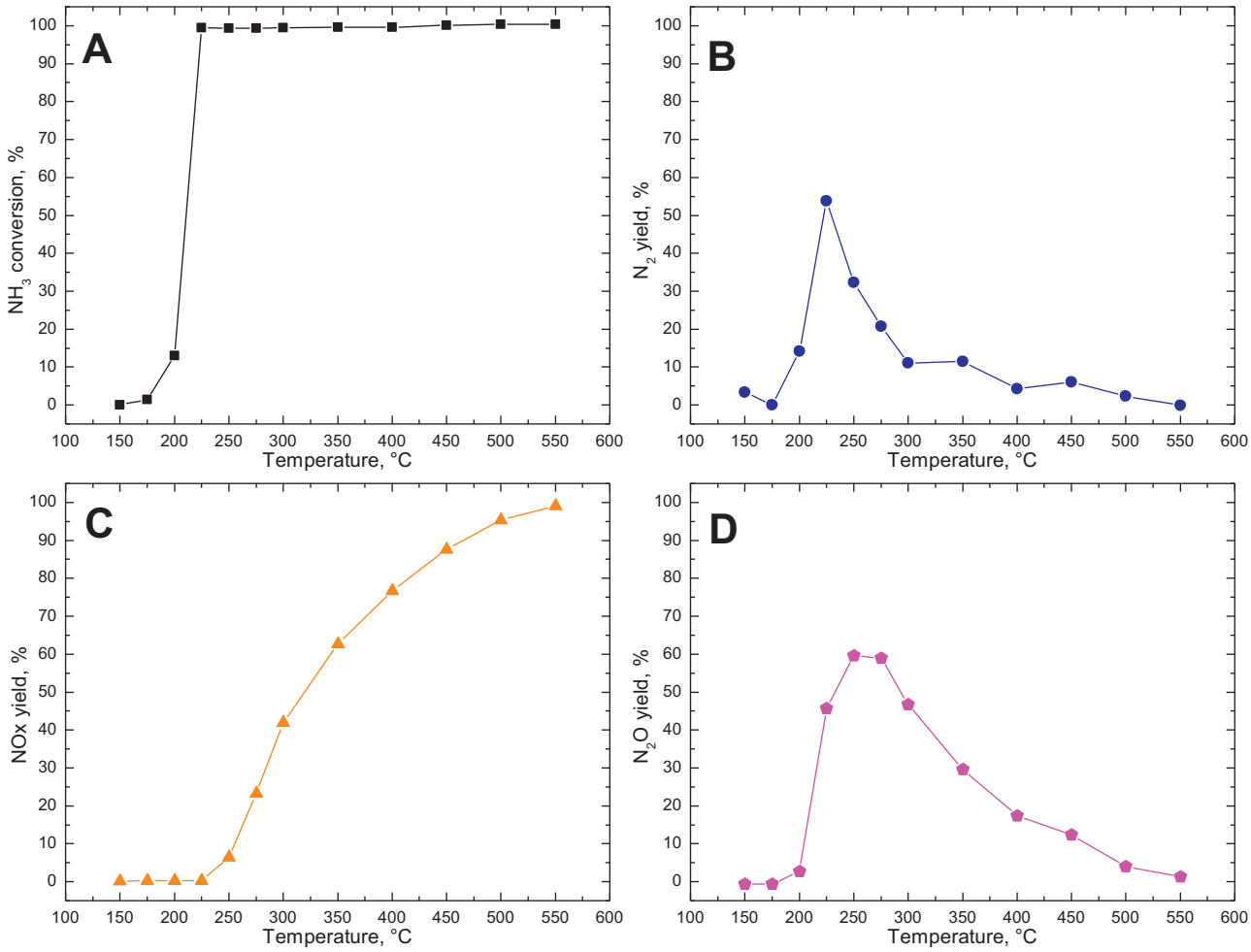

Fig. 2. —NH_3 oxidation on PGM catalyst: NH_3 = 500 ppm; H_2O = 8% (v/v); O_2 = 8% (v/v); carrier gas = He, SV = 1,093,000 $cm^3/h/g_{a.p.}$ (STP).

where:

$$R_i^{TOT} = (1-\chi)\cdot \sum_{k=1}^{nr\text{-SCR}} \upsilon_{i,k} r_k^{SCR} + \chi \cdot \sum_{k=1}^{nr\text{-PGM}} \upsilon_{i,k} r_k^{PGM} \quad (11)$$

$$\chi = \frac{V_{PGM-CAT}}{V_{TOT-CAT}} \quad (12)$$

$$V_{TOT-CAT} = V_{SCR-CAT} + V_{PGM-CAT} \quad (13)$$

Applying the general equations (Eqs. (5)–(7)) (or (Eqs. (8)–(13)) to the relevant chemical species present in the reacting system, a system of partial differential equations (PDE) is obtained. A dedicated FORTRAN code has been used for numerical integration of the PDE system according to the method of lines. The discretization of the variables along the axial coordinate was based on finite differences (FD), using typically a grid with 31 equispaced points. The resulting system of ordinary differential equations was then integrated over time using the LSODI library routine, based on Gear's method for stiff ODEs.

3. Results and discussion

3.1. Identification of the reaction network over the PGM catalyst

3.1.1. NH_3 adsorption–desorption

The ammonia adsorption and desorption properties of the PGM catalyst have been investigated by transient two-stage runs: a TRM run at constant temperature (namely 150 °C), stepwise feeding 500 or 1000 ppm of NH_3 in the presence of water (8%, v/v) and balance helium, was followed by a temperature ramp in order to complete ammonia desorption (TPD).

The experiment (see Fig. A in Supplementary material) showed no evidence of ammonia adsorption onto the catalyst surface during the transient phase. Additionally, the ammonia signal stayed at zero ppm throughout the TPD run, indicating no detectable release of ammonia stored during the adsorption phase. However, the lack of a detectable storage capacity for ammonia (at least under the studied conditions) does not rule out the adsorption of the same species on the catalyst surface:

$$NH_3 + * \leftrightarrow NH_3{}^* \quad (R.1)$$

Indeed, literature reviews on the ammonia oxidation mechanism over PGM catalysts report the unanimous acceptance of reaction steps which consider adsorption of both reactant molecules (NH_3 and O_2) [17]. Moreover, there is general agreement that ammonia adsorbs in on-top position on Pt [18] and that such an adsorption is a non-activated process.

3.1.2. NH_3–O_2

Upon feeding both ammonia and oxygen to the reactor, NH_3 oxidation is expected to proceed, as already widely reported in literature [10,17–19]. N_2, N_2O and NO_x were identified as main oxidation products, with selectivity being a function of the noble metal content and of the catalyst temperature.

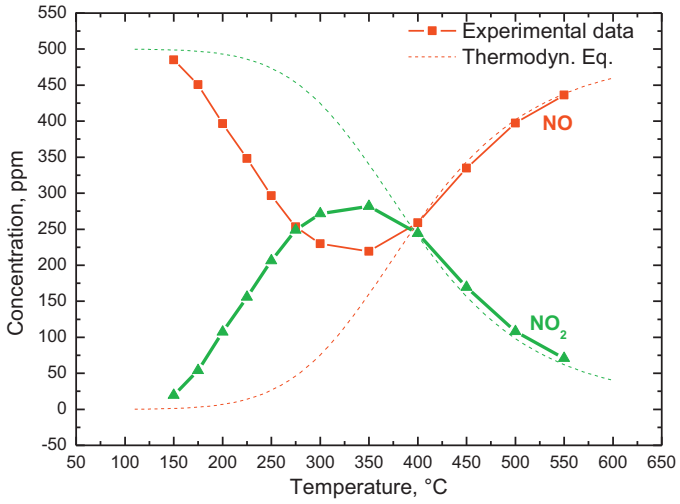

Fig. 3. —NO oxidation on PGM catalyst, steady state data: NO = 500 ppm; H_2O = 8% (v/v); O_2 = 8% (v/v); carrier gas = He, SV = 1,093,000 $cm^3/h/g_{a.p.}$ (STP).

Fig. 2 shows the results collected during steady-state NH_3 oxidation runs performed over the PGM catalyst sample. The feed stream consisted of 500 ppm ammonia in the presence of water (8%, v/v), oxygen (8%, v/v) and balance helium. In Fig. 2A the NH_3 conversion is plotted versus the catalyst temperature, while Fig. 2B–D show respectively the N_2, NO_x ($NO + NO_2$) and N_2O yields for the same tests.

Focusing first on NH_3 conversion (Fig. 2A), a steep reaction light-off was observed between 200 °C and 225 °C, with NH_3 reaching 100% conversion already at 225 °C. The evolution of reaction products started in the same T-window, showing a significant change of products selectivity with temperature. N_2 was the first species to be produced, reaching a maximum yield of about 60% at 225 °C. A further increase of the catalyst temperature resulted then in the progressive decrease of N_2 production. N_2O also showed a maximum behavior, centered around 250 °C. Above 250 °C the NO_x yield started to monotonically increase, reaching a maximum of about 80% at 550 °C. Correspondingly a progressive reduction of both N_2 and N_2O yields was observed. The same test was also repeated with a lower oxygen feed content (2%, v/v, results not shown), showing negligible variations in terms of both NH_3 conversion and N_2, N_2O and NO_x yields. Notably, in spite of the same amount of NO_x produced, the relative proportions of NO and NO_2 were significantly different in the two tests, being controlled by the NO oxidation reaction (R.5).

Species outlet concentrations in the studied temperature range are consistent with the stoichiometry of the following global reactions, which proceed in parallel and prevail at different temperatures, in line with previous literature indications [10,17,18]:

$$2NH_3 + 3/2O_2 \rightarrow N_2 + 3H_2O \quad (R.2)$$

$$2NH_3 + 2O_2 \rightarrow N_2O + 3H_2O \quad (R.3)$$

$$2NH_3 + 5/2O_2 \rightarrow 2NO + 3H_2O \quad (R.4)$$

$$NO + 1/2O_2 \leftrightarrow NO_2 \quad (R.5)$$

3.1.3. NO–O_2

A set of experimental runs was dedicated to study the catalyst behavior in the presence of NO and O_2: steady state activity tests feeding to the reactor NO (500 ppm), O_2 (8%, v/v), H_2O (8%, v/v) and balance helium were performed in the 150–550 °C temperature range. Fig. 3 shows steady-state species outlet concentrations measured during one of such runs: NO started to be converted at 150 °C

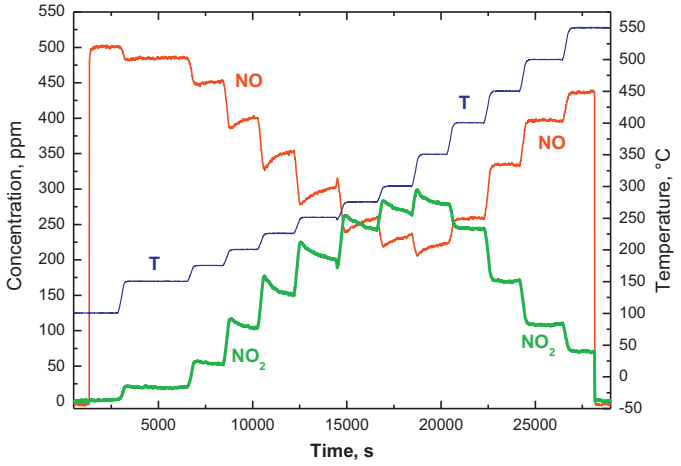

Fig. 4. —NO oxidation on PGM catalyst, transient runs: NO = 500 ppm; H_2O = 8% (v/v); O_2 = 8% (v/v); carrier gas = He, SV = 1,093,000 $cm^3/h/g_{a.p.}$ (STP).

giving NO_2 as the only reaction product and reaching a maximum consumption of about 300 ppm around 350 °C.

It is well known in literature [20] that noble metals are active in the oxidation of NO according to the reversible reaction:

$$NO + 1/2O_2 \leftrightarrow NO_2 \quad (R.5)$$

and the concentration traces in Fig. 3 are consistent with the stoichiometry reported above. Since reaction (R.5) is reversible, the theoretical concentration levels of NO and NO_2 calculated according to the thermodynamic equilibrium constraints are also shown in Fig. 3 (dashed lines). It is evident that below 400 °C the NO conversion is kinetically limited, being far from the equilibrium values. On the opposite, outlet NO and NO_2 concentrations consistent with thermodynamic equilibrium constraints are approached above 400 °C, resulting in a decrease of NO conversion as the temperature is increased.

An interesting feature of NO oxidation over the investigated PGM catalytic system was highlighted during catalyst heat-up transients. Fig. 4 shows the temporal evolution of species outlet concentrations and temperature for the T-steps run whose steady-state values were plotted in Fig. 3. Between 175 and 250 °C, as soon as the catalyst temperature was stepwise increased, the NO trace

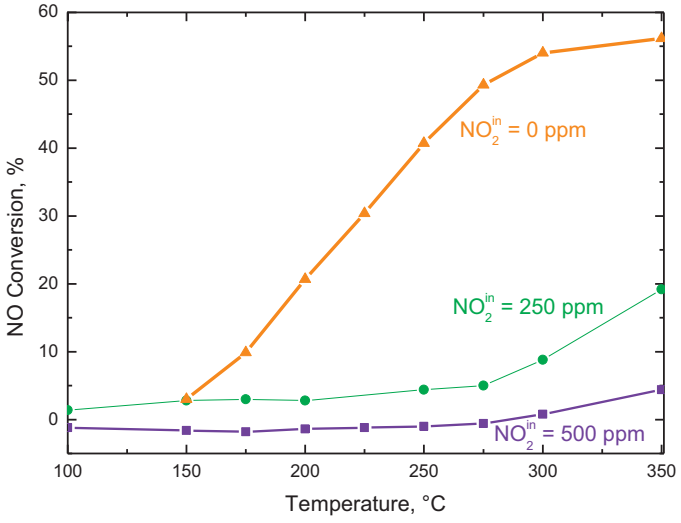

Fig. 5. —NO oxidation on PGM catalyst, NO_2 concentration effect: NO = 500 ppm; NO_2 = 0-250-500 ppm; H_2O = 8% (v/v); O_2 = 8% (v/v); carrier gas = He, SV = 1,093,000 $cm^3/h/g_{a.p.}$ (STP).

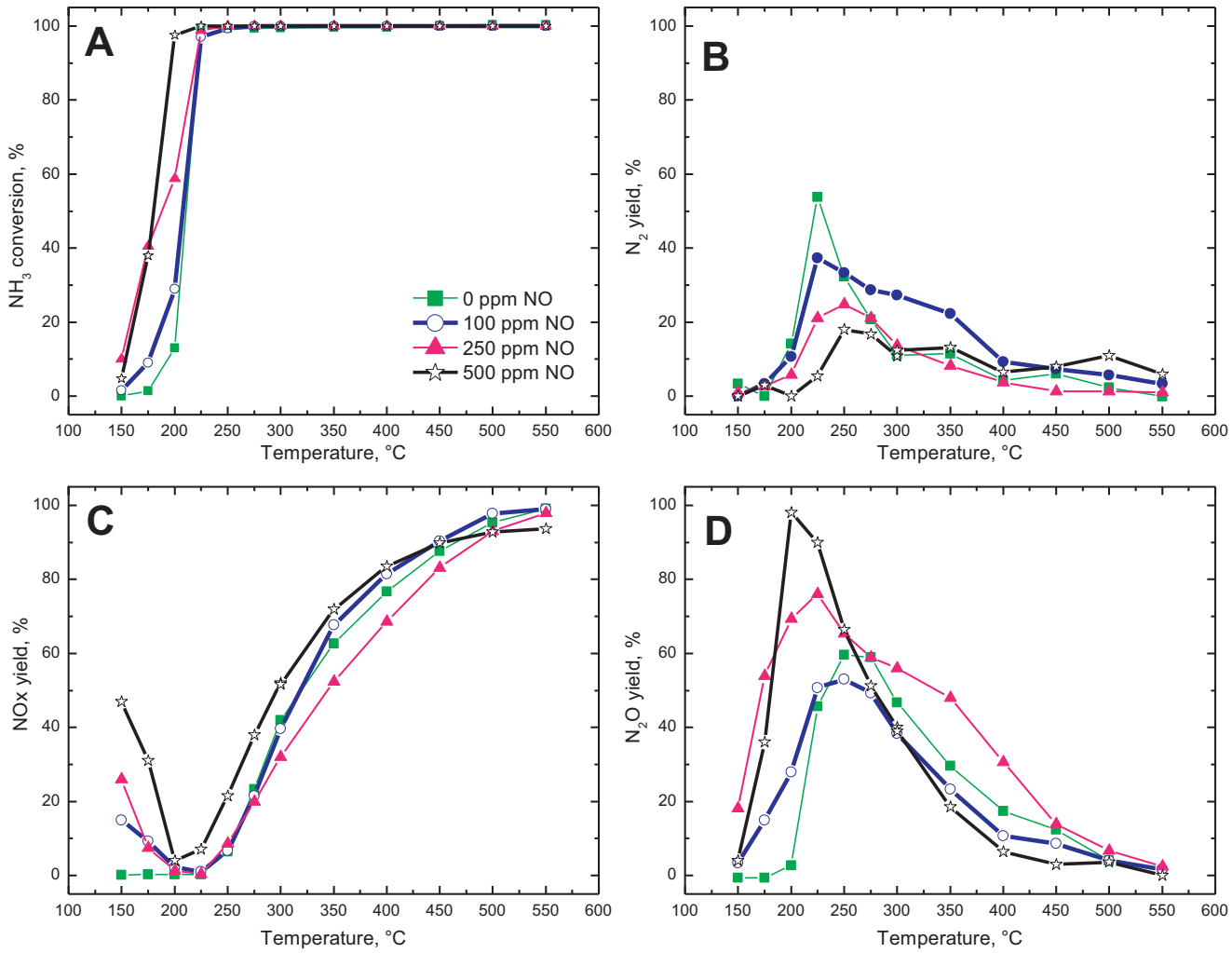

Fig. 6. —NH_3/NO reacting system on PGM catalyst, NO concentration effect: NH_3 = 500 ppm; NO = 0-100-250-500 ppm, NO_2/NO_x = 0; H_2O = 8% (v/v); O_2 = 8% (v/v); carrier gas = He, SV = 1,093,000 $cm^3/h/g_{a.p.}$ (STP).

suddenly dropped with a simultaneous evolution of NO_2. Immediately thereafter, however, although the temperature was kept constant and a steady-state behavior was expected, the NO signal started slowly but steadily to rise again, while the release of NO_2 correspondingly decreased.

According to the literature on transient experiments performed on noble metal systems similar to the present PGM catalyst [20], the slow decrease in NO oxidation activity is ascribed to the strongly oxidizing nature of NO_2, which is responsible for the formation of noble metal oxides/chemisorbed oxygen on the catalyst surface, reducing the catalyst activity. The decreasing NO conversion is thus a result of the NO_2 formed during the reaction, which oxidizes the Pt catalyst. The dynamic behavior observed during the NO oxidation run in Fig. 4 is hence in accordance with literature evidence.

In order to collect further evidence on the role of NO_2 in slowing down the NO oxidation rate, steady-state NO oxidation experiments with 500 ppm NO, 8% (v/v) O_2 and 8% (v/v) H_2O were performed at different NO_2 feed contents, namely 250 ppm and 500 ppm. For each run, the steady-state NO conversions are plotted versus temperature in Fig. 5. Since NO_2 decomposition to NO occurs above 350 °C, only data up to 350 °C are shown. It is observed that the steady-state NO conversion decreases with increasing NO_2, especially in the high temperature range: significant NO_2 inhibition of the NO oxidation activity is thus clearly established.

3.1.4. NH_3—NO—O_2

The effect of NO on NH_3 oxidation was studied in steady state runs where NO (100–250–500 ppm) was fed to the reactor together with 500 ppm of NH_3, 8% (v/v) O_2, 8% (v/v) H_2O and balance helium.

Results of such tests are compared in Fig. 6 with those obtained in the absence of NO in the feed stream (green square dots). The figure shows the comparison in terms of NH_3 conversion (Fig. 6A) and N_2, NO_x and N_2O yields (Fig. 6B–D, respectively).

The addition of increasing amounts of NO to the feed stream had a great impact on both NH_3 conversion and products yields. In the low temperature range (T < 250 °C) increasing the NO feed content drastically promoted the NH_3 conversion, which was limited to less than 15% at 200 °C in the absence of NO, but approached 100% when co-feeding 500 ppm of NO (Fig. 6A). This means a drop of about 50 °C of the reaction light-off temperature in comparison with the NH_3—O_2 reacting system. However, the N_2 yield (Fig. 6B) progressively decreased below 275 °C with the addition of increasing amounts of NO, indicating a greater formation of undesired oxidation products: in particular, the N_2O yield showed indeed an opposite trend, growing with the NO feed content (Fig. 6D). This experimental evidence is well supported by the literature [10,17,18]. The enhanced N_2O production in the presence of NO was

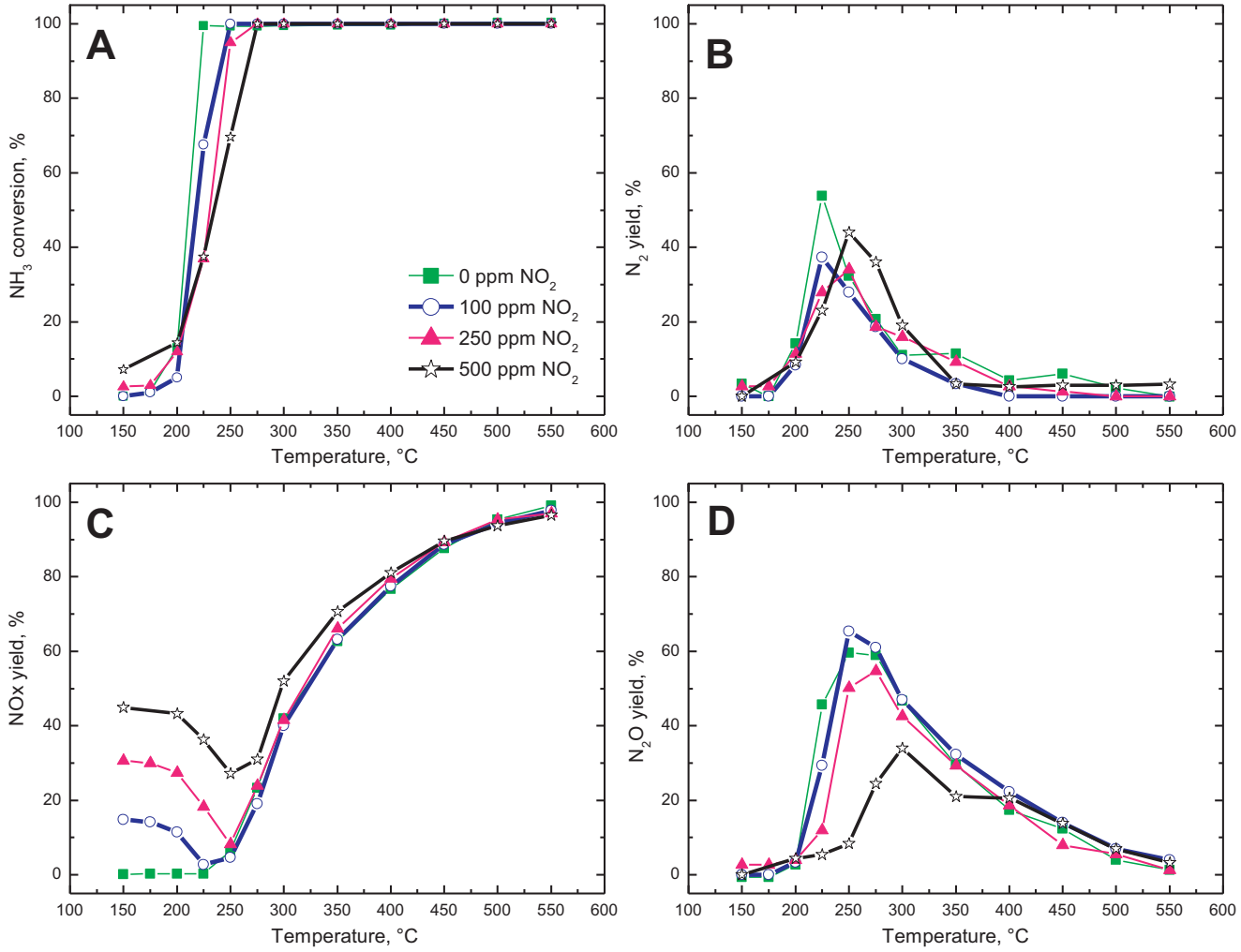

Fig. 7. —NH_3/NO_2 reacting system on PGM catalyst, NO_2 concentration effect: NH_3 = 500 ppm; NO_2 = 0-100-250-500 ppm, NO_2/NO_x = 1; H_2O = 8% (v/v); O_2 = 8% (v/v); carrier gas = He, SV = 1,093,000 $cm^3/h/g_{a.p.}$ (STP).

attributed to the occurrence of the following unselective Standard-SCR reaction:

$$2NH_3 + 2NO + 3/2O_2 \rightarrow 2N_2O + 3H_2O \quad (R.6)$$

A different behavior was observed at high temperatures, namely above 400 °C, with the N_2 and N_2O yields not significantly affected by NO addition. Finally, the trend of NO_x yield as a function of temperature (Fig. 6C) highlights that NO was consumed at low temperatures (150–225 °C T-range) and produced at higher ones, up to 550 °C, where the NO_x yield exceeded 90% independently of the NO feed content. Summarizing, the main finding associated with the analysis of N_2 and NO_x yields as a function of temperature is that the N_2O production was highly enhanced below 275 °C in the presence of NO.

3.1.5. NH_3—NO_2—O_2

NO_2 is commonly present in the feed stream to mobile SCR converters due to the inclusion of an upstream preoxidation catalyst in the configuration of aftertreatment systems. In addition, under unfavorable operative conditions NO_2 might undergo an incomplete selective reduction by NH_3: therefore, it could also represent a possible side product at the outlet of the SCR converter. Hence, being NO_2 a likely component of the ASC feed mixture, the investigation of the NH_3/NO_2 reacting system was also included in the present work.

Fig. 7 shows the experimental results obtained feeding 500 ppm of NH_3 and alternatively 100–250–500 ppm of NO_2 to the reactor while flowing oxygen (8%, v/v), water (8%, v/v) and balance helium. Temperature steps were performed while continuously feeding the mentioned reactant mixture. Experimental results are also compared with those obtained in the absence of NO_2 in the feed stream (green square dots).

The addition of NO_2 to the feed resulted in a lower consumption of NH_3 (Fig. 7A) in the 200–275 °C temperature range. Complete conversion of NH_3 was indeed approached at 225 °C in the absence of NO_2, while total conversion was achieved only at 275 °C when co-feeding also 500 ppm of NO_2. Above this temperature complete ammonia conversion was approached for all reacting mixtures. The N_2 yield was also influenced by the presence of NO_2 (Fig. 7B): the addition of 100 ppm of NO_2 apparently suppressed N_2 formation, with a decrease of the maximum yield from about 60% down to about 40%. However, nitrogen evolution resulted enhanced by greater concentrations of NO_2, with a shift of the maximum yield to higher temperatures with growing NO_2 feed contents. Above 300 °C almost the same yield was obtained both in the presence and in the absence of NO_2. Fig. 7C shows how NO_x, actually NO_2, was partially consumed at temperatures as high as 250 °C; on further increasing the catalyst temperature the NO_x yield monotonically increased independently of the feed mixture composition, approaching almost 100% at 550 °C. The formation of N_2O (Fig. 7D) showed instead a progressive decrease with increasing NO_2 feed

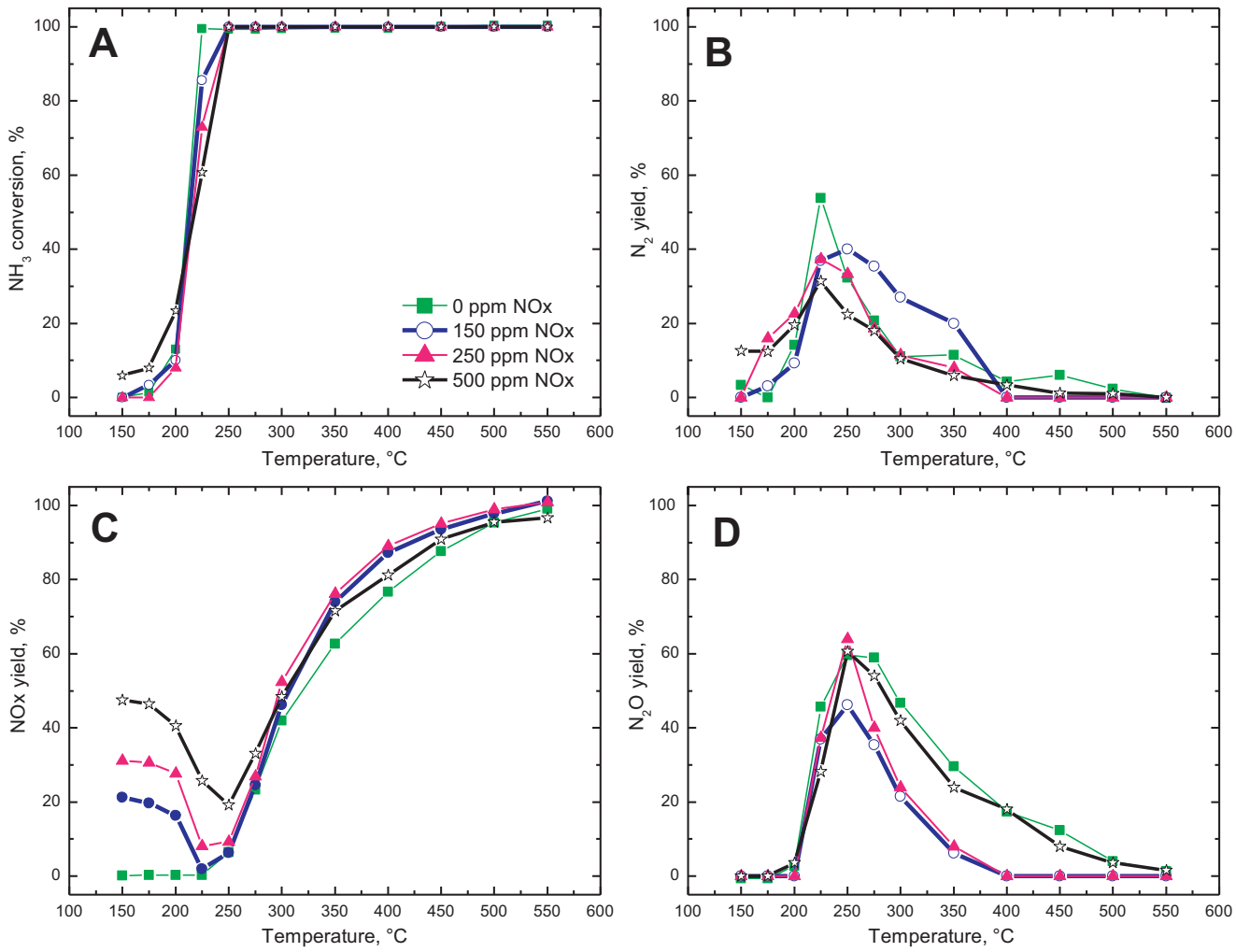

Fig. 8. —NH_3/NO_x reacting system on PGM catalyst, NO_x concentration effect: NH_3 = 500 ppm; NO_x = 0-150-250-500 ppm, NO_2/NO_x = 0.5; H_2O = 8% (v/v); O_2 = 8% (v/v); carrier gas = He, SV = 1,093,000 $cm^3/h/g_{a.p.}$ (STP).

content: a maximum yield of about 30% at 300 °C was recorded in the presence of 500 ppm of NO_2, against a maximum of about 60% in the absence of NO_2. At high temperatures ($T > 400$ °C), in analogy with what observed for the N_2 yield, the amount of produced N_2O seemed to be independent of NO_2.

From the analysis of NH_3 conversion and products yields we can speculate that the NH_3 oxidation reactions were inhibited by NO_2, specifically in the low-T region ($T < 275$ °C), resulting in a decrease of the NH_3 conversion with increasing NO_2 feed contents. The experimental evidence of such an inhibition effect was clear, but a detailed mechanistic study of this phenomenon was not in the scope of this study and will be performed in the next future.

In addition to the inhibited NH_3 oxidation reactions, the NO_x consumption observed in the low-T range justified the introduction of two additional reactions describing the reactivity between NH_3 and NO_2:

$$2NH_3 + 2NO_2 \rightarrow N_2O + N_2 + 3H_2O \quad (R.7)$$

$$4NH_3 + 3NO_2 \rightarrow 7/2N_2 + 6H_2O \quad (R.8)$$

The occurrence of these reactions was independent of the oxygen presence in the feed stream, as verified performing a diagnostic test in the absence of oxygen (results not shown).

3.1.6. NH_3—NO—NO_2—O_2

Finally, the complete $NH_3/NO/NO_2$—O_2 reacting system was also investigated in steady state runs: 500 ppm of NH_3 were fed to the reactor together with 150–250-500 ppm of NO_x (NO_2/NO_x = 0.5), 8% (v/v) O_2, 8% (v/v) H_2O and balance helium. Temperature steps were performed while continuously feeding the mentioned reactants mixture.

Fig. 8 shows collected experimental results in terms of NH_3 conversion (Fig. 8A), N_2 yield (Fig. 8B), NO_x yield (Fig. 8C) and N_2O yield (Fig. 8D) in comparison with results collected in the absence of NO_x in the feed stream (green square dots). Fig. 8A shows that the addition of increasing amounts of NO_x had only a slight impact on the NH_3 conversion, with a slight decrease of catalyst activity in the 200–250 °C temperature region. NO_x had negligible effects on the N_2 yield over the whole T-range (Fig. 8B). The NO_x yield (Fig. 8C) shows a trend similar to those observed for the NH_3/NO and NH_3/NO_2 reacting systems: NO_x were partially consumed at temperatures below 250 °C, then on further increasing the catalyst temperature the NO_x yield monotonically increased independently of the feed mixture composition, approaching 100% at 550 °C. Regarding N_2O formation (Fig. 8D), the highest yields were recorded either in the absence of NO_x or in the presence of the highest NO_x feed content (500 ppm), with a maximum centered around 250 °C.

In summary, it seems that in the low-T region ($T < 275\,^{\circ}C$) NO_2 inhibits both the NH_3 oxidation reactions and the reactivity between NH_3 and NO (reaction R.6). Indeed, the activity enhancement provoked by NO in the feed mixture, as pointed out by Fig. 6, was not observed in the presence of NO_2. Furthermore, there was no direct evidence of additional reactions with respect to those identified during the investigation of the NH_3—O_2, NH_3/NO/O_2 and NH_3/NO_2/O_2 reacting systems.

3.2. Kinetic model for the PGM catalyst

Based on the experimental data analyzed in Section 3.1, the following global reaction network was identified for the NH_3/O_2/NO—NO_2 reactivity over the PGM component of the studied ASC system:

NH_3 adsorption/desorption: $NH_3 + * \leftrightarrow NH_3{}^*$ (R.1)

NH_3 oxidation to N_2: $2NH_3{}^* + 3/2O_2 \rightarrow N_2 + 3H_2O$ (R.2)

NH_3 oxidation to NO: $2NH_3{}^* + 5/2O_2 \rightarrow 2NO + 3H_2O$ (R.4)

NO oxidation to NO_2: $NO + 1/2O_2 \leftrightarrow NO_2$ (R.5)

Non-Selective Standard SCR: $2NH_3{}^* + 2NO + 3/2O_2 \rightarrow 2N_2O + 3H_2O$ (R.6)

NH_3/NO_2 to N_2 and N_2O: $2NH_3{}^* + 2NO_2 \rightarrow N_2 + N_2O + 3H_2O$ (R.7)

NO_2-SCR to N_2: $4NH_3{}^* + 3NO_2 \rightarrow 7/2N_2 + 6H_2O$ (R.8)

Based on this set of reactions, a consistent global kinetic model was developed, as presented and discussed in the following.

3.2.1. NH_3 adsorption/desorption

In a first attempt of model development, as the experimental data presented in Section 3.1 showed negligible ammonia adsorption capacity onto the PGM catalyst, the description of adsorption phenomena was avoided. However this resulted in the incorrect description of catalyst activity in the high temperature regime, where NH_3 adsorption likely becomes rate controlling for the oxidation reactions [10]. For this reason, and in line with literature evidence [17,18], ammonia adsorption was assumed to proceed on Pt sites as a non-activated and molecular process, while an Arrhenius rate law was used to describe the desorption process. Accordingly, the following rate equations were adopted:

NH_3 adsorption: $r_{ads} = k_{ads-PGM} C_{NH_3} \left(1 - \theta_{NH_3}^{PGM}\right)$ (14)

NH_3 desorption: $r_{des} = \exp\left[k_{des\text{-}PGM}^0 - E_{des\text{-}PGM}\left(\frac{1000}{T} - \frac{1000}{473}\right)\right] \cdot \theta_{NH_3}^{PGM}$ (15)

Notably, a re-parameterized form of the desorption rate constant was used, with the purpose of reducing correlation of the rate parameter estimates during parameter fitting. The same re-parameterized form of the rate constant was also implemented in all the rate equations defined in the following paragraphs.

3.2.2. NH_3 oxidation and non-selective standard SCR

Three reactions, namely (R.2), (R.4) and (R.6), were included in the kinetic model to describe the reactivity between NH_3 and O_2, both in the presence and in the absence of NO.

For the three reactions we assumed first order kinetics with respect to the NH_3 surface coverage, and a negative dependence on the NO_2 concentration. Experimental runs performed over the PGM catalyst showed indeed that NH_3 oxidation as well as the reactivity between NH_3 and NO are both inhibited by NO_2, which could be present either as the product of NO oxidation or as a component of the feed mixture. Indeed, a detailed mechanistic investigation of the NO_2 inhibition phenomenon was beyond the scope of the PGM kinetic model development. In view of our current lack of understanding, we have therefore chosen a purely empirical approach in order to describe NO_2 inhibition of the kinetics. Accordingly, we introduced LHHW-type terms in the denominators of rate Eqs. (16)–(18), thus accounting for their negative order dependence on the NO_2 concentration, without however necessarily invoking the competitive adsorption of NH_3 and NO_2 on the same catalytic site. Such inhibition terms thus are not associated with a single NO_2 adsorption constant, but rather with multiple fitting parameters.

Additionally, the assumed kinetics were zero order with respect to oxygen, based on the observed negligible variations of catalyst activity and products selectivity over the 2%–8% (v/v) O_2 concentration range. Finally, for reaction R.6 first order kinetics were considered with respect to the NO gas phase concentration,

$$\text{NH}_3\text{ oxidation to } N_2: \quad r_{NN} = \frac{\exp\left(k_{NN}^0 - E_{NN}(1000/T - 1000/473)\right) \cdot \theta_{NH_3}^{PGM}}{\left(1 + K_{NN} \cdot C_{NO_2}\right)} \tag{16}$$

$$\text{NH}_3\text{ oxidation to NO}: \quad r_{NO} = \frac{\exp\left(k_{NO}^0 - E_{NO}(1000/T - 1000/473)\right) \cdot \theta_{NH_3}^{PGM}}{\left(1 + K_{NO} \cdot C_{NO_2}\right)} \tag{17}$$

$$\text{NH}_3/\text{NO}/O_2\text{ to } N_2O: \quad r_{NHNOOX} = \frac{\exp\left(k_{NHNOOX}^0 - E_{NHNOOX}(1000/T - 1000/473)\right) \cdot \theta_{NH_3}^{PGM} C_{NO}}{\left(1 + K_{NHNOOX} \cdot C_{NO_2}\right)} \tag{18}$$

It is worth emphasizing that Fig. 2, as well as literature data on PGM catalysts, show formation of N_2O from NH_3 oxidation also in the absence of NO in the feed stream. Notwithstanding such experimental and literature evidence, no direct pathway from $NH_3 + O_2$ to N_2O was considered in the herein developed kinetic scheme. The sum of (R.4) and (R.6) results however in the stoichiometry of NH_3 oxidation to N_2O:

$2NH_3^* + 5/2O_2 \rightarrow 2NO + 3H_2O$ (R.4)

$NH_3^* + NO + 3/4O_2 \rightarrow N_2O + 3/2H_2O$ (R.6)

$2NH_3^* + 2O_2 \rightarrow N_2O + 3H_2O$ (R.3)

The present reaction scheme can thus in principle describe also the N_2O formation observed in the absence of NO in the feed stream.

3.2.3. NO oxidation

The oxidation of NO to NO_2 is a reversible reaction, well studied in the literature over PGM catalytic systems [21–23]. Different rate expressions as well as mechanistic studies can be traced in the literature on this topic. Two main aspects characterize the kinetics of this reaction: the first one is that thermodynamic equilibrium constraints must be respected, the second one is that a strong inhibiting effect of NO_2 on the NO oxidation over PGM systems

has been extensively reported [21,22]. In line both with literature evidence and with the collected data, a consistent reaction rate was adopted (Eq. (19)), which takes into account both the equilibrium constraints and the aforementioned inhibiting effect of NO_2:

$$\text{NO oxidation to } NO_2: \quad r_{NOox} = \exp\left(k^0_{NOox-PGM} - E_{NOox-PGM}\left(\frac{1000}{T} - \frac{1000}{473}\right)\right) \times \frac{\left(C_{NO}\sqrt{P_{O_2}} - C_{NO_2}/K^{eq}_{NO_2}\right)}{\left(1 + K_{NO_2-PGM}\cdot C_{NO_2}\right)} \tag{19}$$

3.2.4. Reactions involving NH_3 and NO_2

Two reactions were included in the kinetic model to account for the reactivity of NH_3 with NO_2:

$$NH_3/NO_2 \text{ to } N_2 \text{ and } N_2O: \quad 2NH^*_3 + 2NO_2 \rightarrow N_2 + N_2O + 3H_2O \tag{R.7}$$

$$NO_2 - \text{SCR to } N_2: \quad 4NH^*_3 + 3NO_2 \rightarrow 7/2N_2 + 6H_2O \tag{R.8}$$

Second order overall kinetics in ammonia surface coverage and NO_2 gas phase concentration were adopted for both reactions (R.7)

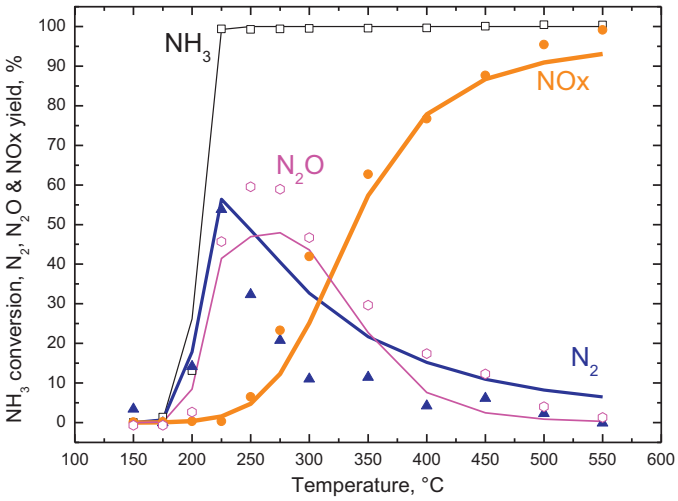

Fig. 9. NH_3 oxidation on PGM catalyst, kinetic fit: NH_3 = 500 ppm; H_2O = 8% (v/v); O_2 = 8% (v/v); carrier gas = He, SV = 1,093,000 $cm^3/h/g_{a.p.}$ (STP). Symbols: experimental results; lines: model fit.

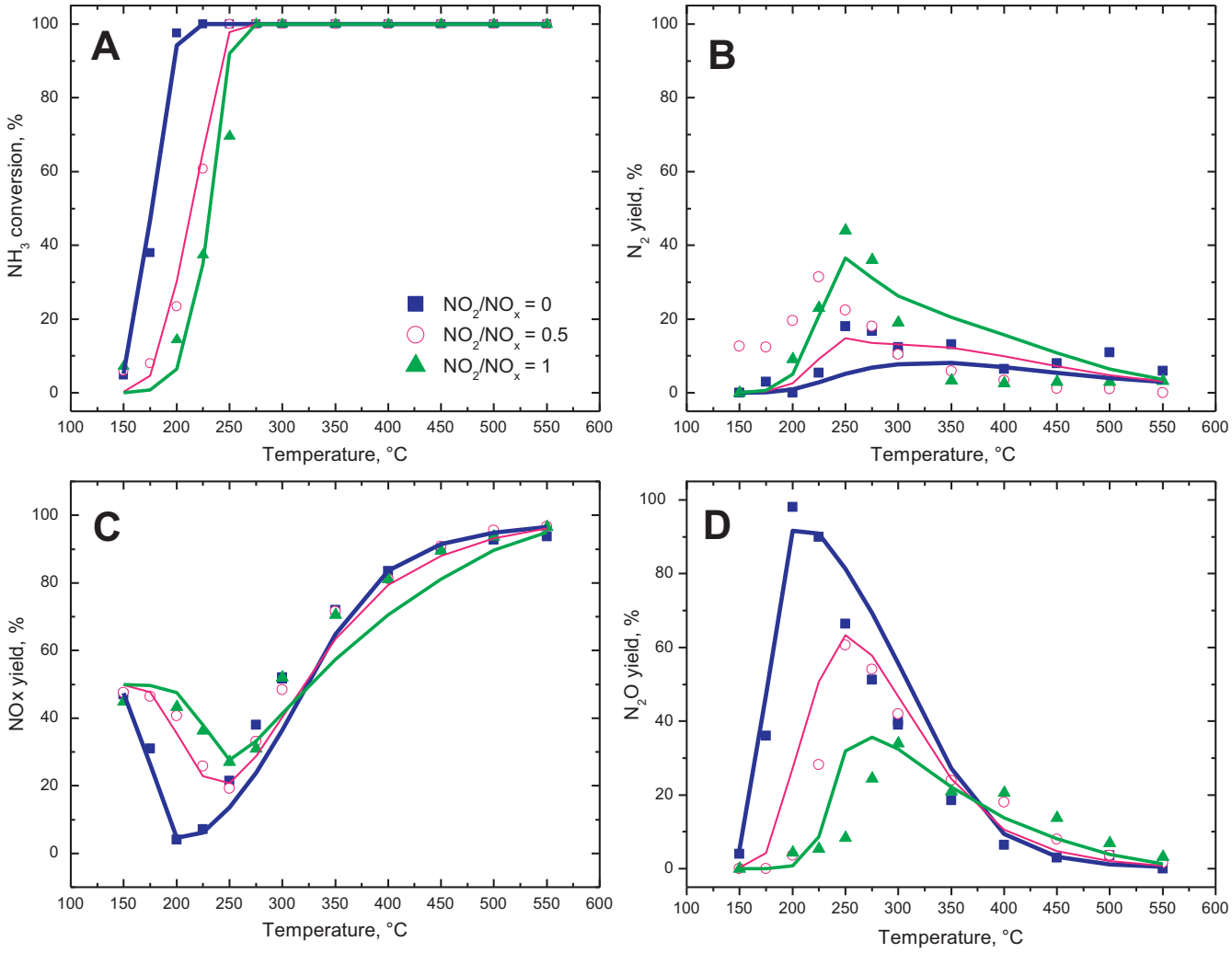

Fig. 10. —NH_3/NO—NO_2 reacting system on PGM catalyst, effect of NO_2/NO_x ratio and kinetic fit for alpha = 1: NH_3 = 500 ppm; NO_x = 500 ppm; NO_2/NO_x = 0, 0.5, 1; H_2O = 8% (v/v); O_2 = 8% (v/v); carrier gas = He, SV = 1,093,000 $cm^3/h/g_{a.p.}$ (STP). Symbols: experimental results; lines: model fit.

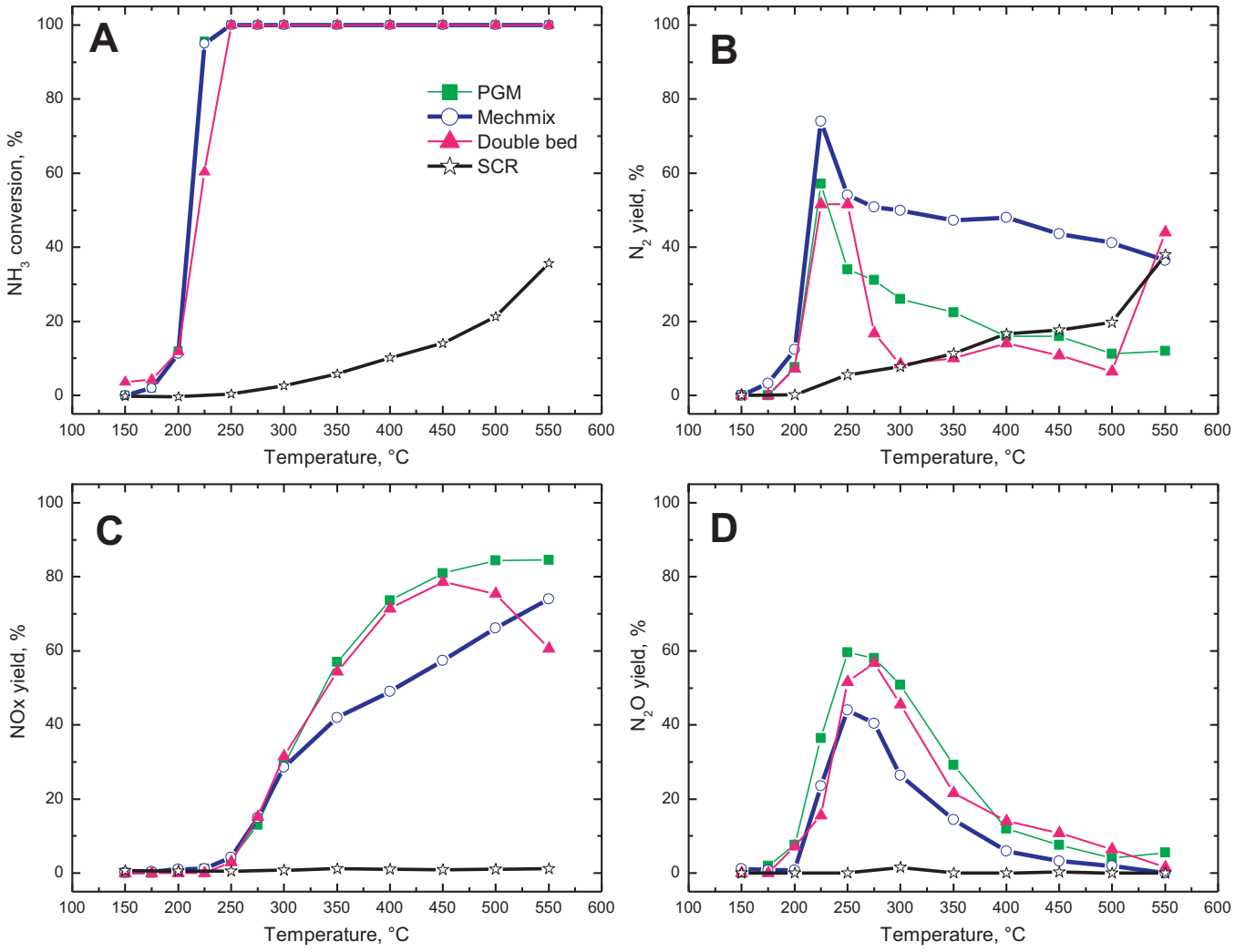

Fig. 11. —NH_3 oxidation, comparison of different reactor configurations: NH_3 = 500 ppm; H_2O = 8% (v/v); O_2 = 8% (v/v); carrier gas = He. SV^{PGM} = 1,093,000 $cm^3/h/g_{a.p.}$ (STP), SV^{SCR} = 690,000 $cm^3/h/g_{a.p.}$ (STP).

and (R.8). This resulted in similar rate equations, namely (Eqs. (20) and (21)).

$$\mathrm{NH_3/NO_2\ to\ N_2\ and\ N_2O:}\quad r_{NHNOO} = \exp\left(k^0_{NHNOO} - E_{NHNOO}\left(\frac{1000}{T} - \frac{1000}{473}\right)\right)\cdot\theta^{PGM}_{NH_3}C_{NO_2} \tag{20}$$

$$\mathrm{NO_2-SCR\ to\ N_2:}\quad r_{NOO} = \exp\left(k^0_{NOO} - E_{NOO}\left(\frac{1000}{T} - \frac{1000}{473}\right)\right)\cdot\theta^{PGM}_{NH_3}C_{NO_2} \tag{21}$$

Reactions (R.1), (R.2) and (R.4)–(R.8), with the related rate equations (Eqs. (14)–(21)), thus provide a global kinetic scheme for the PGM component of the investigated ASC system.

3.3. Kinetic fit

Experimental data collected over the powdered PGM catalysts have been analyzed according to the heterogeneous one-dimensional plug-flow dynamic reactor model described in Section 2. Rate parameters of (Eq. (19)) were independently estimated from NO oxidation tests while a global multiresponse non-linear regression based on the least squares method applied to the whole set of runs involving NH_3 provided estimates of the remaining rate parameters in Eqs. (14)–(21).

Kinetic fit results are presented in Figs. 9 and 10. Fig. 9 refers to the NH_3 oxidation runs, where experimental (symbols) and calculated (solid line) ammonia conversion and N_2, N_2O and NO_x yields are plotted versus the catalyst temperature. The model provides a fairly good description of the data over the whole 150–550 °C T-range. The onset of NH_3 conversion is indeed well captured as well as the evolution of products yields as a function of catalyst temperature. Minor deviations can be observed between 250 °C and 300 °C for the N_2 yield and above 400 °C for the NO_x yield.

For the NO—O_2 reacting system (see Fig. B in Supplementary material) the model was able to describe the experimentally observed trend of steady-state NO conversions over the whole investigated temperature range, both in the kinetically (T < 400 °C) and in the thermodynamically (T > 400 °C) controlled regimes.

Fig. 10 illustrates the effects of the NO_2/NO_x feed ratio on NH_3 conversion and N_2, NO_x and N_2O yields when feeding to the PGM catalysts equimolar amounts of NH_3 and NO_x (α = 1). Experimental

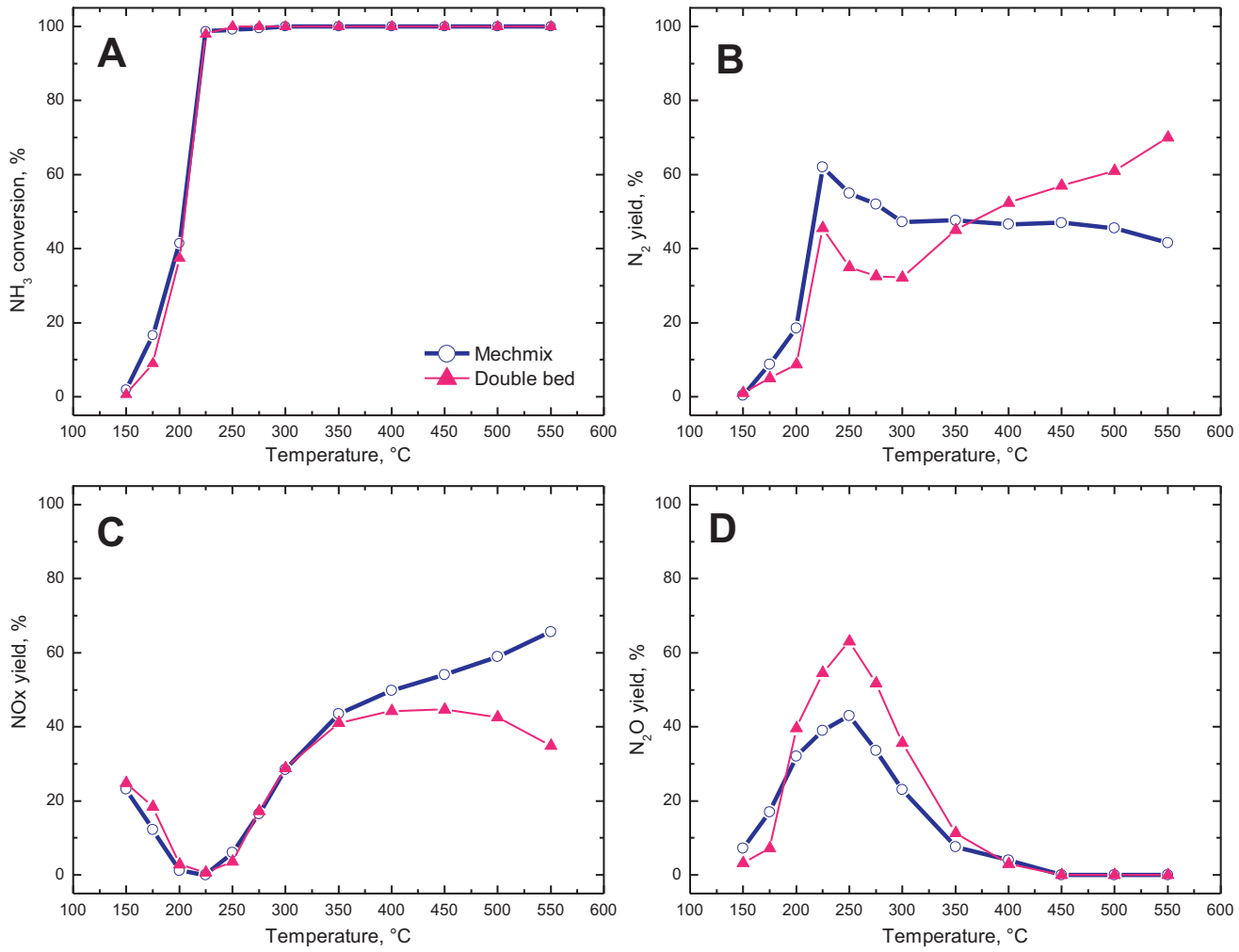

Fig. 12. —NH_3/NO reacting system on SCR + PGM catalysts, Double Bed versus Mechanical Mixture: NH_3 = 750 ppm; NO = 250 ppm; H_2O = 8% (v/v); O_2 = 8% (v/v); carrier gas = He, SV^{PGM} = 1,093,000 $cm^3/h/g_{a.p.}$ (STP). SV^{SCR} = 690,000 $cm^3/h/g_{a.p.}$ (STP).

data (symbols) are plotted versus temperature together with fit results (solid lines).

The effect of the NO_2/NO_x ratio in terms of NH_3 conversion is well captured by the model, with a decrease of catalyst activity on increasing the NO_2 content. The qualitative trends of N_2, NO_x and N_2O yields are also well captured as a function of both temperature and NO_2/NO_x ratio, though the quantitative agreement is not always perfect. Some deviations can indeed be observed below 275 °C for NO_2/NO_x = 0.5 and above 300 °C for NO_2/NO_x = 1.

The same qualitative results are observed also in case of excess ammonia in the feed stream (see Fig. C in Supplementary material for fit results with α = 5).

3.4. Analysis of SCR/PGM interaction

As discussed in Section 2, the dual-layer ASC configuration involves the presence of a PGM catalytic layer beneath the SCR coating. A micro-flow reactor loaded with powder is inherently unsuitable for reproducing the real ASC system configuration: above all, no arrangement of catalytic beds exists which can effectively simulate the NO_x back-diffusion and reaction with the ammonia pre-adsorbed on the SCR catalyst. Accordingly, the fundamental study performed over SCR-PGM combined systems definitely does not claim to faithfully simulate the real ASC system behavior. The aim of this investigation was rather to elucidate experimentally the interactions between the SCR and the PGM catalytic chemistries in relation to limiting (segregated versus mixed) spatial arrangements of the two catalysts. Two catalytic bed layouts have been in fact designed to achieve these goals: (i) a Double Bed configuration, with the first bed and the second bed consisting of the SCR catalyst and of the PGM catalyst, respectively, provides information on the sequential combination of the respective catalytic activities; (ii) a single bed configuration, wherein the reactor is loaded with a mechanical mixture of the two catalyst powders, can suitably provide experimental evidence of local parallel interactions between the catalytic chemistries.

Like for the PGM catalyst, both the "Double Bed" and "Mechanical Mixture" configurations were studied by means of steady state runs addressing the main SCR reacting systems, namely NH_3/O_2, $NH_3/NO/O_2$, $NH_3/NO_2/O_2$ and $NH_3/NO—NO_2/O_2$.

3.4.1. $NH_3—O_2$

In order to figure out the role that the combination of different catalysts plays on reactivity and selectivity of ammonia oxidation, Fig. 11 compares data collected over the SCR catalyst only, the PGM catalyst only and over the two SCR/PGM combined systems. The analysis is based on NH_3 conversion, N_2, NO_x and N_2O yields obtained when feeding to the catalysts 500 ppm of NH_3, 8% (v/v) O_2, 8% (v/v) H_2O and balance Helium.

Observing the data in Fig. 11, it is clearly apparent that the catalyst composition dramatically affects both the ammonia oxidation activity and the products selectivity. The SCR catalyst shows the

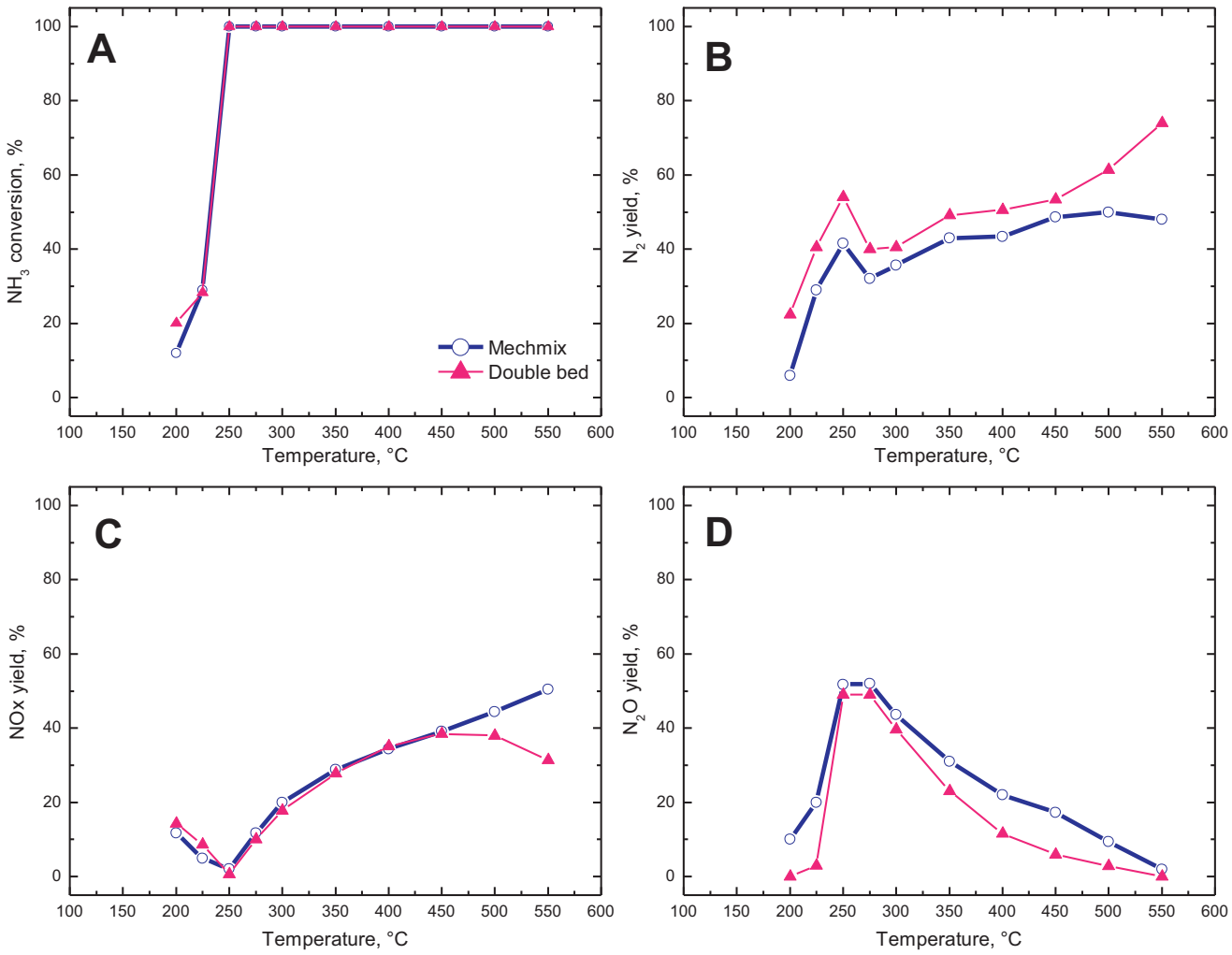

Fig. 13. —NH_3/NO_2 reacting system on SCR + PGM catalysts, Double Bed versus Mechanical Mixture: NH_3 = 750 ppm; NO_2 = 250 ppm; H_2O = 8% (v/v); O_2 = 8% (v/v); carrier gas = He. SV^{PGM} = 1,093,000 $cm^3/h/g_{a.p.}$ (STP). SV^{SCR} = 690,000 $cm^3/h/g_{a.p.}$ (STP).

weakest oxidation performance, resulting in incomplete ammonia oxidation with almost total selectivity towards N_2 at all temperatures, as well-established in the literature for Fe-zeolite SCR catalysts [3,7,8,24].

On the opposite, the PGM catalyst exhibits the highest ammonia oxidation activity, with NH_3 conversion above 90% already at 200 °C (Fig. 11A). However the same catalyst is also the one associated with the highest yield of NO_x in the high T-range (see Fig. 11C).

When the SCR catalyst is followed by the PGM one ("Double Bed" configuration), the overall activity is strengthened due to the presence of the PGM catalyst: NH_3 conversion and products yields are indeed almost overlapped with those of the PGM only catalyst below 300 °C, with some deviations only in terms of N_2 yield. However, on moving to higher temperatures the contribution of the upstream SCR layer becomes significant, as pointed out by the increased N_2 yield above 500 °C (Fig. 11B) and the corresponding decrease of the NO_x yield (Fig. 11C). This trend is likely related to the partial selective conversion of NH_3 to N_2 in the SCR catalyst bed. As a result a lower amount of unreacted ammonia is available for the oxidation to NO occurring in the following PGM bed.

The best compromise between activity and selectivity was achieved with the PGM/SCR mechanical mixture: complete NH_3 conversion was indeed obtained already at 275 °C, with N_2 yields above 40% over the whole 150–550 °C T-range. Correspondingly, lower NO_x and N_2O yields compared with PGM catalyst only and Double Bed configuration were measured between 300 °C and 500 °C.

The direct comparison between the two ASC combined systems (Double Bed versus Mechanical Mixture) points out how the mechanical mixture of SCR and PGM powders entails the occurrence of interactions between the chemistries prevailing over the catalysts, which instead do not take place in the Double Bed configuration where the two catalysts are segregated. The different selectivity observed in the simultaneous presence of both catalysts are due in fact to the competition between the SCR and PGM reactivities, as the SCR reaction products can react over the PGM catalyst and vice versa. A similar picture was observed by Long et al. [25] who studied a noble metal promoted Fe-ZSM-5 for Selective Catalytic Oxidation of NH_3. Long et al. [25] attributed the reduced N_2O and NO_x production to the SCR features of the combined catalyst: N_2O and NO generated by NH_3 oxidation over the noble metal can be indeed further reduced to N_2 by unreacted ammonia, thus improving simultaneously both ammonia conversion and N_2 selectivity.

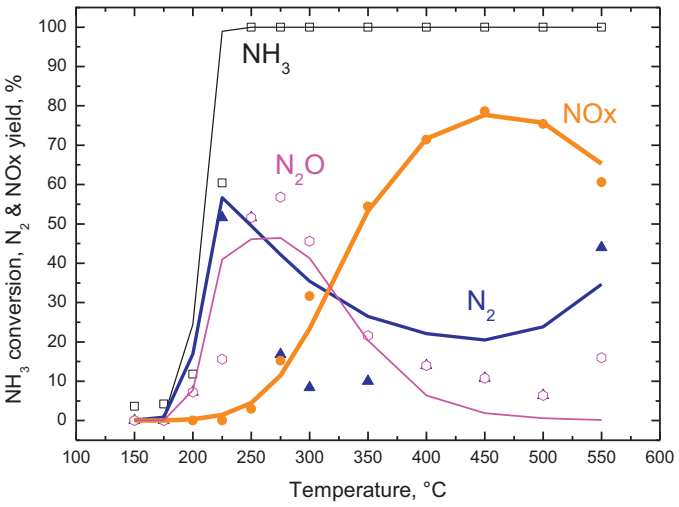

Fig. 14. —NH_3 oxidation on Double Bed (SCR + PGM) configuration, model simulations: NH_3 = 500 ppm; H_2O = 8% (v/v); O_2 = 8% (v/v); carrier gas = He. SV^{PGM} = 1,093,000 $cm^3/h/g_{a.p.}$ (STP). SV^{SCR} = 690,000 $cm^3/h/g_{a.p.}$ (STP). Symbols: experimental results; lines: model simulations.

3.4.2. NH_3—NO_x—O_2

The combined SCR/PGM systems were comparatively analyzed in terms of steady state activity and products yields in the case of a feed mixture composed of 750 ppm of NH_3, 250 ppm of NO_x, 8% (v/v) O_2, 8% (v/v) H_2O and balance Helium. The comparisons of NH_3 conversion, N_2, NO_x and N_2O yields are shown for NO_2/NO_x feed ratios of 0 (Fig. 12) and 1 (Fig. 13). For NO_2/NO_x of 0.5 refer to Fig. D in Supplementary material.

For all NO_2/NO_x ratios no significant differences between "Double bed" and "mechanical mixture" configurations were apparent in terms of NH_3 conversion. On the opposite, the different arrangement of the two catalysts in the reactor played a role in determining products yields. In terms of N_2 yields the picture was complicated and varied depending on the NO_2/NO_x feed ratio. In the case of NO_2/NO_x = 0 (Fig. 12B), a higher N_2 yield was recorded over the mechanical mixture below 350 °C, while at higher temperatures the Double Bed configuration prevailed. A constantly higher N_2 yield over the Double Bed (Fig. 13B) was also recorded in the case of NO_2/NO_x = 1.

Focusing on the NO_x yield, a common qualitative trend is shown independently of the NO_2/NO_x ratio (Figs. 12C and 13C): at low temperatures the Double Bed and Mechanical mixture configurations exhibited the same NO_x yields, while at high temperatures (above 350 °C or 450 °C depending on the NO_2/NO_x ratio) the lower

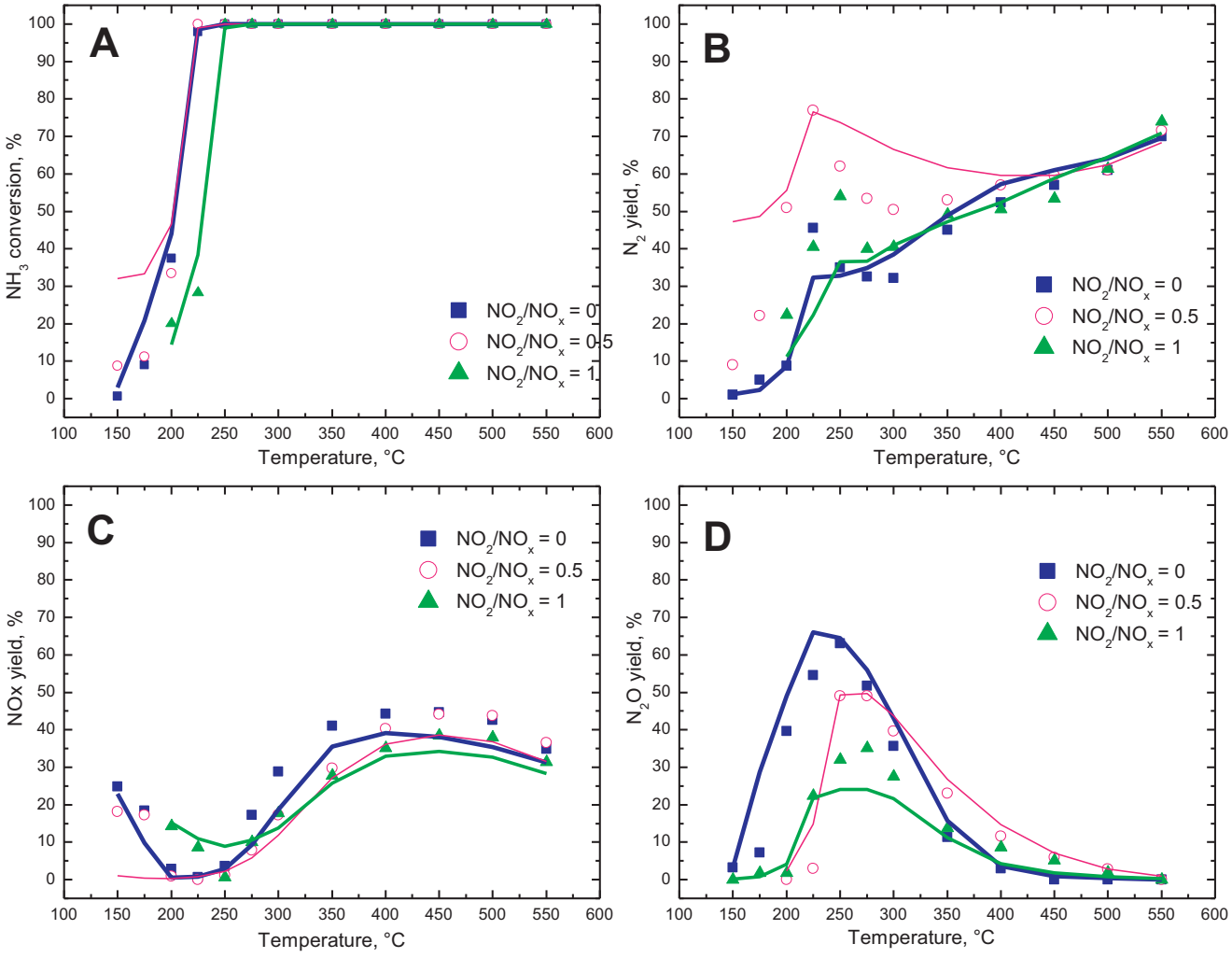

Fig. 15. —NH_3/NO—NO_2 reacting system on Double Bed (SCR + PGM) configuration, effect of NO_2/NO_x ratio, model simulations: NH_3 = 750 ppm; NO_x = 250 ppm; H_2O = 8% (v/v); O_2 = 8% (v/v); carrier gas = He. SV^{PGM} = 1,093,000 $cm^3/h/g_{a.p.}$ (STP). SV^{SCR} = 690,000 $cm^3/h/g_{a.p.}$ (STP). Symbols: experimental results; lines: model simulations.

NO_x yields were always obtained in the case of the Double Bed configuration.

In the high temperature region ($T > 350\,^{\circ}C$), the general decrease of the NO_x yield in favor of the N_2 yield over the Double Bed configuration was likely related to the occurrence of the NH_3-SCR reactions in the upstream SCR bed. The temperature increase boosted indeed the ammonia and NO_x consumption over the SCR catalyst in the Double Bed configuration, providing a reduced ammonia and NO_x supply to the PGM catalyst bed downstream, thus resulting in a reduced NO_x evolution.

Finally, the effect of the reactor configuration on the N_2O yield resulted to be a function of the NO_2/NO_x feed ratio: when NO was the only source of NO_x (Fig. 12D) the mechanical mixture exhibited a lower N_2O yield in the whole 150–550 °C T-range in comparison with the Double Bed configuration. The latter system showed however lower N_2O yields when NO_2 was present in the feed stream (Fig. 13D).

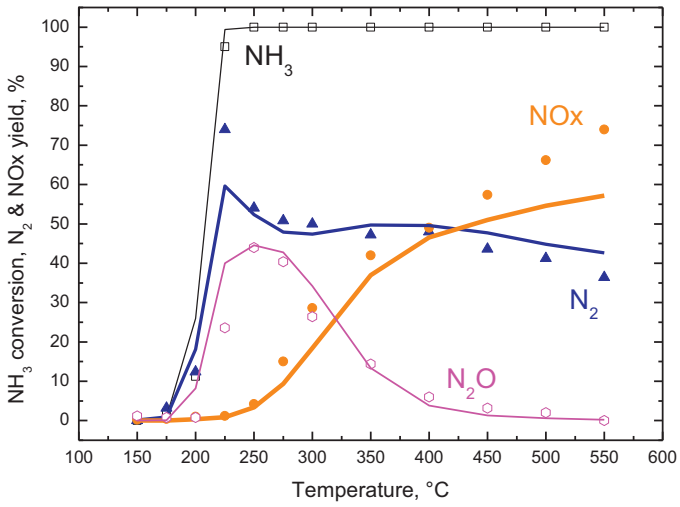

Fig. 16. —NH_3 oxidation on Mechanical Mixture (SCR + PGM) configuration, model simulations: NH_3 = 500 ppm; H_2O = 8% (v/v); O_2 = 8% (v/v); carrier gas = He. SV^{PGM} = 1,093,000 $cm^3/h/g_{a.p.}$ (STP). SV^{SCR} = 690,000 $cm^3/h/g_{a.p.}$ (STP). Symbols: experimental results; lines: model simulations.

3.5. *Predictive simulations of SCR/PGM combined systems*

Experimental data collected over both Double Bed and Mechanical mixture configurations were systematically compared with predictive model simulations, as shown in Figs. 14–17. The simulations were generated simply assuming the superposition of the SCR

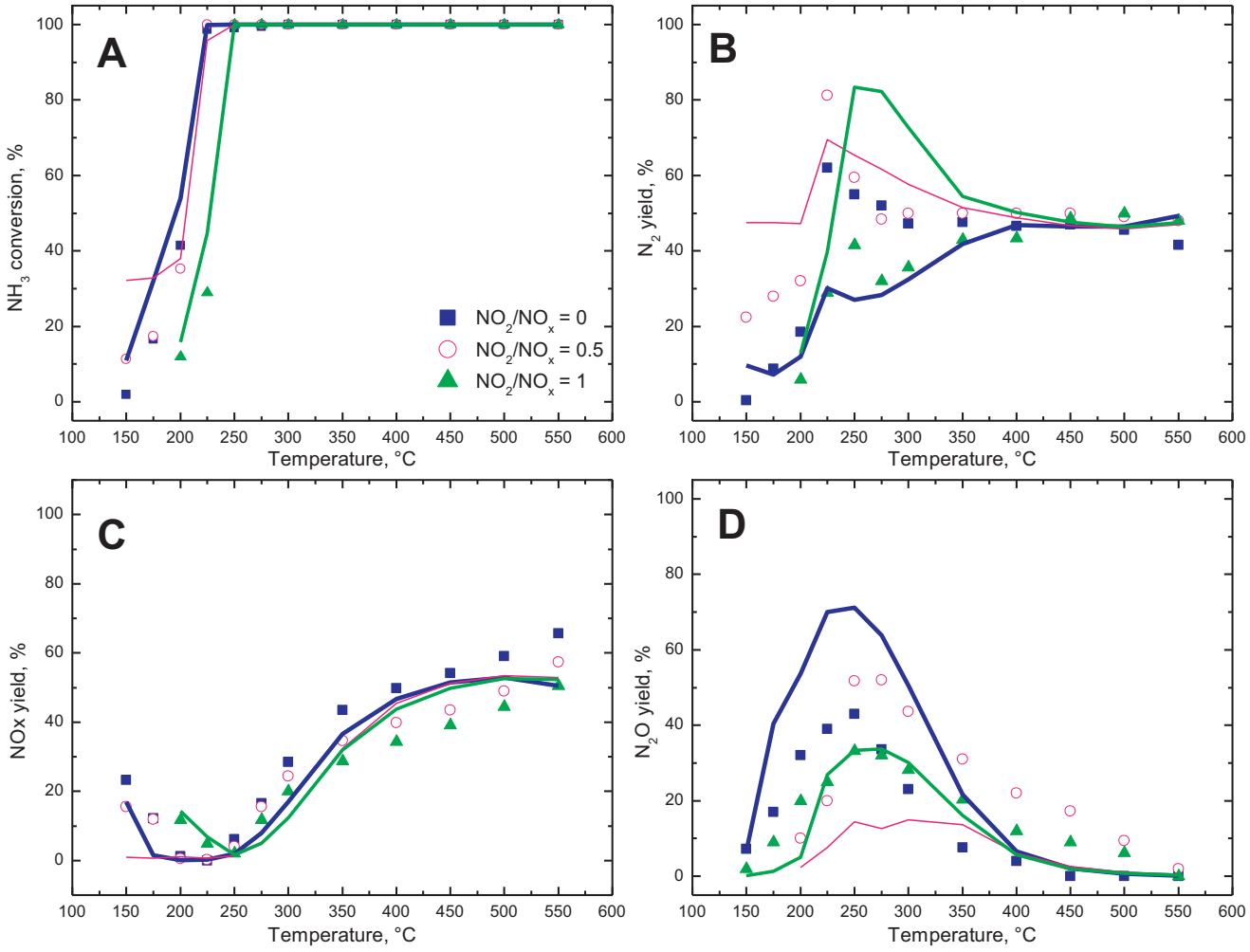

Fig. 17. —NH_3/NO—NO_2 reacting system on Mechanical Mixture (SCR + PGM) configuration, effect of NO_2/NO_x ratio, model simulations: NH_3 = 750 ppm; NO_x = 250 ppm; H_2O = 8% (v/v); O_2 = 8% (v/v); carrier gas = He. SV^{PGM} = 1,093,000 $cm^3/h/g_{a.p.}$ (STP). SV^{SCR} = 690,000 $cm^3/h/g_{a.p.}$ (STP). Symbols: experimental results; lines: model simulations.

and PGM kinetics independently determined over the two powdered catalyst components of the ASC system.

Fig. 14 shows simulation results for the Double Bed configuration in the case of the NH_3/O_2 reacting system. A good match between experimental data (symbols) and simulations (solid lines) is evident for both ammonia conversion and NO_x yield, while some deviations are present between 275 °C and 500 °C for the N_2 and N_2O yields.

For the same configuration, the effect of NO_2/NO_x is shown in Fig. 15. Simulations (solid lines) resulted in good agreement with experiments (symbols) in the whole T-range for NO_2/NO_x feed ratios of either 0 or 1. In the case of $NO_2/NO_x = 0.5$ a good match between experiments and simulations was found above 275 °C, while in the low-T range the overestimation of catalyst activity (Fig. 15A, pink line vs. diamonds) resulted in the somewhat incorrect prediction of N_2 and NO_x yields (Fig. 15B and C, pink line vs. diamonds).

Predictive simulations of NH_3 conversion and products yields in the case of the mechanical mixture configuration are shown in Fig. 16 for the NH_3/O_2 reacting system. In this case model predictions resulted in very good agreement with experimental data over the whole 150–550 °C T-range, but for minor deviations of the NO_x yield above 450 °C.

A good simulation quality is also apparent above 350 °C in Fig. 17, showing the effect of the NO_2/NO_x ratio on NH_3 conversion and products yields for the mechanical mixture. Significant deviations in terms of N_2 and N_2O yields were instead observed comparing model predictions and experimental data below 350 °C, specifically in the case of $NO_2/NO_x = 0$ and 1.

On the whole, the results in Figs. 14–17 emphasize that the overall performance of combined SCR + PGM systems results from a simple superposition of the respective catalytic chemistries, which however provides different results depending on the relative spatial distribution of the two catalyst components.

4. Conclusions

As a part in the development and validation of a chemically and physically consistent mathematical model of a commercial dual-layer (SCR + PGM) monolithic NH_3 slip converter (ASC), we have reported in this paper on $NH_3/O_2/NO—NO_2$ steady-state and transient kinetic runs performed over the PGM component of the NH_3 slip catalyst, herein tested in the form of precursor washcoat powders. From these data an original global PGM kinetic model was developed, which fully accounts for the effects of temperature and of NO_x co-feed (with variable NO_2/NO_x feed ratio in the 0–1 range) on NH_3 oxidation. The model considers both the well known NO_2 inhibition of NO oxidation, as well as a novel NO_2 inhibition effect on the NH_3 oxidation reactions. The fit reveals that NH_3 adsorption becomes the rate limiting step at intermediate-high temperatures.

Comparative $NH_3/O_2/NO—NO_2$ steady-state runs were performed also over two different combinations of SCR + PGM powders, loaded in the test micro-reactor either as a sequential double-bed or as a mechanical mixture, respectively. While the NH_3 oxidation activity was similar, being controlled by the PGM component, the N_2 selectivity was greater over the mechanical mixture, due to the fact that in this configuration the unselective NH_3 oxidation products (NO_x) formed over the PGM catalyst had a chance to further react selectively with more NH_3 over the SCR catalyst. Such a positive interaction between the PGM and the SCR catalytic chemistries was satisfactorily predicted by a model involving the simple superposition of the PGM and SCR kinetics.

In summary, the present preliminary fundamental study has confirmed a positive interaction between SCR and PGM catalytic chemistries, which beneficially affects the N_2 selectivity. This promising synergy needs to be further verified in the real dual-layer monolith configuration of the ASC system. Accordingly, in the following part of the project the herein developed PGM kinetics, together with consistent SCR kinetics, are incorporated in a novel dual-layer monolith catalyst model, and validated against both lab-scale and engine test bench data collected over dual-layer ASC catalysts. The related results will be reported in a forthcoming paper.

Appendix A. Supplementary data

Supplementary data associated with this article can be found, in the online version, at http://dx.doi.org/10.1016/j.apcatb.2012.10.031.

References

[1] T.V. Johnson, SAE Technical Paper 2011-01-0304 (2011).
[2] A. Scheuer, W. Hauptmann, A. Drochner, J. Gieshoff, H. Vogel, M. Votsmeier, Applied Catalysis B: Environmental 111–112 (2012) 445–455.
[3] M. Colombo, I. Nova, E. Tronconi, V. Schmeißer, B. Bandl-Konrad, L. Zimmermann, Applied Catalysis B: Environmental 111–112 (2011) 106–118.
[4] M. Iwasaki, K. Yamazaki, H. Shinjoh, Applied Catalysis A: General 366 (2009) 84–92.
[5] P. Markatou, J. Dai, A. Johansson, W. Klink, M. Castagnola, T.C. Watling, M. Tutuianu, SAE Technical Paper 2011-01-1304 (2011).
[6] L. Olsson, H. Sjövall, R.J. Blint, Applied Catalysis B: Environmental 87 (2009) 200–210.
[7] A. Schuler, M. Votsmeier, P. Kiwic, J. Gieshoff, W. Hautpmann, A. Drochner, H. Vogel, Chemical Engineering Journal 154 (2009) 333–340.
[8] H. Sjövall, R.J. Blint, A. Gopinath, L. Olsson, Industrial & Engineering Chemistry Research 49 (2010) 39–52.
[9] D. Chatterjee, T. Burkhardt, M. Weibel, I. Nova, A. Grossale, E. Tronconi, SAE Technical Paper 2007-01-1136 (2007).
[10] A. Scheuer, M. Votsmeier, A. Schuler, J. Gieshoff, A. Drochner, H. Vogel, Topics in Catalysis 52 (2009) 1847–1851.
[11] A. Scheuer, O. Hirsch, R. Hayes, H. Vogel, M. Votsmeier, Catalysis Today 175 (2011) 141–146.
[12] M. Colombo, I. Nova, E. Tronconi, Chemical Engineering Science 75 (2012) 75–83.
[13] C. Ciardelli, I. Nova, E. Tronconi, M. Ascherfeld, W. Fabinski, Topics in Catalysis 42–43 (2007) 161–164.
[14] C. Ciardelli, I. Nova, E. Tronconi, B. Konrad, D. Chatterjee, K. Ecke, M. Weibel, Chemical Engineering Science 59 (2004) 5301–5309.
[15] P.L. Villa, P. Forzatti, G. Buzzi-Ferraris, G. Garone, I. Pasquon, Industrial & Engineering Chemistry Process Design and Development 24 (1985) 12–19.
[16] G. Buzzi-Ferraris, G. Donati, Chemical Engineering Science 29 (1974) 1504–1509.
[17] R. Kraehnert, M. Baerns, Chemical Engineering Journal 137 (2008) 361–375.
[18] E.V. Rebrov, M.H.J.M. de Croon, J.C. Schouten, Chemical Engineering Journal 90 (2002) 61–76.
[19] Y. Li, J.N. Armor, Applied Catalysis B: Environmental 13 (1997) 131–139.
[20] D. Bhatia, R.W. McCabe, M.P. Harold, V. Balakotaiah, Journal of Catalysis 266 (2009) 106–119.
[21] W. Hauptmann, M. Votsmeier, J. Gieshoff, A. Drochner, H. Vogel, Applied Catalysis B: Environmental 93 (2009) 22–29.
[22] L. Olsson, E. Fridell, Journal of Catalysis 210 (2002) 340–353.
[23] L. Olsson, H. Persson, E. Fridell, M. Skoglundh, B. Andersson, The Journal of Physical Chemistry B 105 (2001) 6895–6906.
[24] K. Kamasamudram, N.W. Currier, X. Chen, A. Yezerets, Catalysis Today 151 (2010) 212–222.
[25] R.Q. Long, R.T. Yang, Catalysis Letters 78 (2002) 353–357.